

# **Novel Approach for Welding Stainless Steel Using Cr-Free Welding Consumables**

**Final Report**

G.S. Frankel\* and J.C. Lippold\*\*

\*Fontana Corrosion Center, Dept. of Materials Science and Engineering

\*\*Dept. of Industrial, Welding and Systems Engineering

The Ohio State University, Columbus, OH 43210

SERDP Project PP-1346

December 31, 2004



# Report Documentation Page

*Form Approved*  
*OMB No. 0704-0188*

Public reporting burden for the collection of information is estimated to average 1 hour per response, including the time for reviewing instructions, searching existing data sources, gathering and maintaining the data needed, and completing and reviewing the collection of information. Send comments regarding this burden estimate or any other aspect of this collection of information, including suggestions for reducing this burden, to Washington Headquarters Services, Directorate for Information Operations and Reports, 1215 Jefferson Davis Highway, Suite 1204, Arlington VA 22202-4302. Respondents should be aware that notwithstanding any other provision of law, no person shall be subject to a penalty for failing to comply with a collection of information if it does not display a currently valid OMB control number.

1. REPORT DATE <b>31 DEC 2004</b>		2. REPORT TYPE <b>Final</b>		3. DATES COVERED <b>-</b>	
4. TITLE AND SUBTITLE <b>Novel Approach for Welding Stainless Steel Using Cr-Free Welding Consumables</b>				5a. CONTRACT NUMBER	
				5b. GRANT NUMBER	
				5c. PROGRAM ELEMENT NUMBER	
6. AUTHOR(S) <b>G.S. Frankel* and J.C. Lippold**</b>				5d. PROJECT NUMBER <b>PP 1346</b>	
				5e. TASK NUMBER	
				5f. WORK UNIT NUMBER	
7. PERFORMING ORGANIZATION NAME(S) AND ADDRESS(ES) <b>*Fontana Corrosion Center, Dept. of Materials Science and Engineering **Dept. of Industrial, Welding and Systems Engineering The Ohio State University, Columbus, OH 43210</b>				8. PERFORMING ORGANIZATION REPORT NUMBER	
9. SPONSORING/MONITORING AGENCY NAME(S) AND ADDRESS(ES) <b>Strategic Environmental Research &amp; Development Program 901 N Stuart Street, Suite 303 Arlington, VA 22203</b>				10. SPONSOR/MONITOR'S ACRONYM(S) <b>SERDP</b>	
				11. SPONSOR/MONITOR'S REPORT NUMBER(S)	
12. DISTRIBUTION/AVAILABILITY STATEMENT <b>Approved for public release, distribution unlimited</b>					
13. SUPPLEMENTARY NOTES <b>The original document contains color images.</b>					
14. ABSTRACT					
15. SUBJECT TERMS					
16. SECURITY CLASSIFICATION OF:			17. LIMITATION OF ABSTRACT <b>SAR</b>	18. NUMBER OF PAGES <b>79</b>	19a. NAME OF RESPONSIBLE PERSON
a. REPORT <b>unclassified</b>	b. ABSTRACT <b>unclassified</b>	c. THIS PAGE <b>unclassified</b>			

# 1. Table of Contents

1.	Table of Contents .....	i
2.	List of Acronyms .....	ii
3.	List of Figures .....	iii
4.	List of Tables .....	iii
5.	Acknowledgements .....	1
6.	Executive Summary .....	2
7.	Objective .....	4
8.	Background .....	4
9.	Materials and Methods .....	6
10.	Results and Accomplishments .....	7
11.	Conclusions .....	15
12.	Appendices .....	16

## 2. List of Acronyms

$E_{CORR}$	Corrosion potential
$E_B$	Breakdown potential
$E_{RP}$	Repassivation potential
SS	Stainless steel
SMAW	Shielded metal arc welding
GTAW	Gas tungsten arc welding
PEL	Permissible exposure limit
OSHA	Occupational Safety and Health Administration
SERDP	Strategic Environmental Research and Development Program
OCP	Open circuit potential
AWS	American Welding Society
LTE	Long term exposre
SEM	Scanning Electron Microscopy
EDS	Energy Dispersive Spectroscopy

### 3. List of Figures

Figure 1. High quality Monel/304L weld.	7
Figure 2. 304L/Monel weld after 50 days exposure in aerated artificial seawater.	8
Figure 3. Example of pit formed in 304L/Monel weld after 50 days exposure in artificial seawater.	8
Figure 4. Summary of breakdown and open circuit potentials (OCP) for 304L/Monel weld and a number of other materials in 0.1 M NaCl at the end of 14 days exposure.	9
Figure 5. Effect of Cu content on results from potentiodynamic polarization curves for Ni-Cu alloys and weld in artificial seawater. open symbols – deaerated, closed symbols – aerated. a) open circuit corrosion potential b) breakdown potential.	10
Figure 6. The effect of Pd content on the $E_{CORR}$ and $E_B$ of furnace-cooled and water-quenched 7:3 Ni-Cu alloys in aerated 0.1 M NaCl.	11
Figure 7. The effect of dilution on the $E_{CORR}$ and $E_B$ of furnace-cooled and water-quenched 7:3 Ni-Cu alloys in aerated 0.1 M NaCl.	11
Figure 8. The effect of Cu content on the $E_{CORR}$ , $E_B$ , and $E_{RP}$ of as-cast Ni-Cu alloys with and without 25% dilution in aerated 0.1M NaCl. The values for type 304L stainless steel are shown at left of plot for comparison.	12
Figure 9. The effect of alloying elements of Pd and Mo on the $E_{CORR}$ (a), $E_B$ (b), and $E_{RP}$ (c) of as-cast Ni-10Cu alloys with the dilution of 0%, 25% and 50% in aerated 0.1 M NaCl.	13
Figure 10. Cyclic polarization behavior of type 304L stainless steel, conventional weld of 308L, as-cast Ni-10Cu-1Pd alloy, and Monel in aerated 0.1 M NaCl.	14

### 4. List of Tables

Table 1. Details of GTAW procedure.	7
-------------------------------------	---

## **5. Acknowledgements**

The work in this report was performed primarily by two graduate students at The Ohio State University: Yeong Ho Kim in the Department of Materials Science and Engineering and Gustavo Guaytima in the Department of Industrial, Welding and Systems Engineering. Their tireless efforts are greatly appreciated. Gustavo earned his MS in the summer of 2004 and Yeong Ho is on schedule to finish his PhD in 2005. The PIs also acknowledge the support and guidance provided by the SERDP program office, Chuck Pellerin in particular.

## 6. Executive Summary

This project was a SERDP seed grant that was extended from the normal one year duration to a total of two years. The goal of the project was to demonstrate the feasibility of a new approach for welding stainless steel using Cr-free consumables. Stainless steels are usually selected as a material of construction for their corrosion resistance. When they are fabricated into structures, stainless steel components are often joined by welding. In order to ensure that the welds exhibit sufficient corrosion resistance, filler metals matching or exceeding the chromium (Cr) content of the base metal must be used. The Cr content of Types 304 and 308 stainless steels, the most commonly used stainless steel and the filler metal used to weld, respectively, is 18-20 wt%. Evaporation and oxidation of Cr from the molten weld pool results in emission of carcinogenic hexavalent Cr ( $\text{Cr}^{+6}$  or chromate) in the fumes. This is a significant health hazard for the welders and necessitates considerable expense for ventilation systems. In some conditions relevant to DOD interests, such as cramped ship interiors, it is extremely difficult to ventilate effectively. Furthermore, any future reduction in the Permissible Exposure Limit (PEL) for chromate in welding fume, which is under consideration by OSHA, will exacerbate the situation. It is the objective of this proposal to develop a Cr-free consumable for welding austenitic stainless steel that provides mechanical properties and corrosion resistance comparable to the Cr-bearing consumable that are currently used.

The approach to solving this problem considers that, if stainless steel (SS) is to be welded with a filler metal that is different in composition than the base metal, then the corrosion of the welded structure will be controlled by the phenomenon of galvanic corrosion. Furthermore, passive metals such as stainless steels usually corrode in a localized nature. From this perspective and fundamental concepts in corrosion, it is possible to develop design criteria for the weld consumable, at least regarding the corrosion properties:

1. The breakdown and repassivation potentials of the weld metal should be higher than the corrosion potential of the SS substrate to prevent localized attack of the weld metal.
2. If possible, the corrosion potential of the weld metal should be slightly higher than that of the SS substrate so that the weld metal is cathodically protected.

It should be noted that other important considerations are the mechanical properties of the weld, the weldability, and the stress corrosion cracking behavior. Based on the design criteria and the well-known galvanic series for metals in seawater (which ranks the relative nobility of different metals), Monel-400 was chosen as a starting point for this project. This alloy, which is essentially Ni-30Cu, has good corrosion resistance in seawater and has a corrosion potential close to that of types 304 and 316 stainless steel.

In the course of this project it was shown that good quality gas tungsten arc welds could be achieved using Monel filler metal and Type 304L base metal by controlling shielding gas and weld heat input. The strength and ductility of Monel/304L GTA welds were comparable to those of 308L/304L welds. Weld solidification cracking was observed at high heat inputs and dilution

levels, but could be eliminated by restricting the dilution of base metal in to the consumable below about 30% base metal.

Preliminary fume analysis studies were performed to validate that the use of Cr-free consumables will in fact reduce the Cr content of welding fumes. Type 304L SS plate was welded using an SMAW process with either standard 308L welding rod or the Monel weld rod. The Cr content of the welding fume was  $0.24 \pm 0.12$  wt% Cr for a 19% dilution weld made with a Monel weld rod, and  $3.5 \pm 1.3$  wt% Cr for a standard weld made with a 308L weld rod. So the improvement was more than a factor of 10. The emission was not zero with the Cr-free consumable because Cr from the base metal was diluted into the weld and a portion was entrained in the weld fume. However, this proves that the consumable is the major source of Cr (308L contains 19.5-22 %Cr) and that the emission of Cr is reduced by removing Cr from the consumable.

No corrosion was observed on a 304L/Monel weld sample after long term exposure to 0.1 M NaCl. However, some localized corrosion of the weld was observed after long term exposure to artificial seawater. Sharp line attack was observed at the base-metal/weld-metal interface as a result of compositional dilution and accompanied microstructural heterogeneities. Large and shallow pits were found in the weld metal. Interdendritic regions rich in Cu are attacked during potentiodynamic polarization to high potentials, indicating an increased susceptibility associated with high Cu content.

The effects of alloying additions to Ni-30Cu were investigated. Pd additions in the range of 1-2% had a large influence in increasing the corrosion potential and improving the localized corrosion behavior of Ni-Cu alloys, but the addition of Mo was not effective. Dilution of Ni-Cu with stainless steel up to 15% improved the localized corrosion resistance, but slightly decreased the corrosion potential. Further dilution degraded the corrosion resistance. Considering corrosion properties only, dilution should be kept to the range of less than 20%.

Given the detrimental influence of Cu on the localized corrosion behavior of Ni-Cu alloys, Cu content down to 0% was investigated. It was found that 5-10 wt% Cu was sufficient to increase the corrosion potential, and provided the best resistance to localized corrosion. Alloys with 5 and 10 wt% Cu with small additions of Pd and Mo were also tested. Again it was found that Mo was not beneficial, but that Pd increased the corrosion potential and improved the localized corrosion behavior.

The final “optimized” composition for a Cr-free consumable from a corrosion perspective was Ni-(5-10)Cu-1Pd. This alloy exhibits a corrosion potential that is slightly higher than that of type 304L SS. It has the highest breakdown potential of all the Cr-free alloys studied, though it is lower than that of type 304L SS. On the other hand, the repassivation potential of this alloy is much higher than that of 304L SS. The breakdown and repassivation potentials of this alloy are considerably higher than the corrosion potential of type 304L SS. Therefore, it satisfies the design criteria.

## 7. Objective

There is a wide range of welding processes, most of which involve the formation of a molten metal zone. The very high temperatures in the weld pool result in considerable vaporization of metal and generation of a fume that contains fine particles of metal in various oxidation states. In many cases, weld fumes are an extreme danger to the health of the welder. For welding of stainless steel, of particular interest is the Cr(VI) content (Cr(VI) is chromium in the 6+ oxidation state and is commonly referred to as chromate). Fumes containing Cr(VI) can cause lung cancer. Shielded Metal Arc Welding (SMAW) is a manual welding process used in shipyards. In shipbuilding operations, SMAW of stainless steel is often performed in cramped conditions, such as within the interior of a ship, where ventilation to remove the dangerous fumes is difficult. The problem will become more severe if the Permissible Exposure Limit (PEL) set by the Occupational Safety and Health Administration (OSHA) are lowered. The major source of material for a weld fume is the consumable, although base metal diluted into the weld can also end up in the fume. Clearly it is of interest to limit the generation of dangerous fumes by decreasing the content in the consumable of metals such as Cr and Mn that are dangerous when present in fumes.

The objective of this study is to develop a Cr-free consumable that is compatible with processes for welding stainless steel. From a welding perspective, solidification cracking, intermediate temperature embrittlement, mechanical properties and alloy hot formability need to be understood. The critical corrosion issues include the susceptibility to localized corrosion, dealloying effects during long term exposure, solution flow effects, and environmental cracking.

## 8. Background

Corrosion resistance is the absolute key to developing a successful approach to welding SS with Cr-free consumables, since SS will only be used in corrosive environments. If the welds are susceptible to corrosion, then the liabilities from the fabrication process will negate the benefits of stainless steel.

Stainless steel obtains its corrosion resistance from the addition of Cr; steel becomes stainless when it contains greater than about 12% Cr. The "stainless" nature is a result of the spontaneous formation of an extremely thin (a few nm in thickness) passive film that is very rich in Cr. This passive film is essentially a Cr oxy-hydroxide. The corrosion resistance of SS continues to improve with increasing Cr content, and typical 304 SS contains 18-20% Cr. Nickel is added (8-12%) to stabilize the austenite phase for improved mechanical properties.

The problem with passive metals such as stainless steels and Al alloys is that the passive film is susceptible to localized breakdown and accelerated attack, which can take the form of pits, crevices or cracks (if the material is stressed). Localized corrosion of SS typically occurs in chloride-containing environments. Improvements in localized corrosion resistance are obtained by adding 2-3% Mo to the 304 composition, resulting in 316 SS.

Because of the corrosion susceptibility associated with heat-affected zones and with segregation and second phase formation in the fusion zone, welds are usually the sites of corrosion attack in welded structures. Therefore, it is common to use overalloyed weld filler metal that is rich in Cr. For instance, 304 SS with 18-20% Cr is typically welded with 308 SS consumables with 19-22% Cr. Overalloyed weld filler metals make the hexavalent Cr emission problem worse.

It is possible to eliminate fume generation by utilizing a solid state welding process such as friction welding or friction stir welding. These processes require complete re-engineering of the welding process and are limited in terms of their application. It is the goal of this project to develop a Cr-free filler metal that would be a drop-in replacement for conventional SS welding consumables.

#### Basis for design: fundamentals of localized corrosion and galvanic corrosion

If SS is to be welded with a filler metal that is different in composition, then the corrosion of the welded structure will be controlled by galvanic corrosion. Furthermore, the mode of corrosion of passive metals such as stainless steels is usually localized in nature, such as in pitting corrosion. Therefore, to understand the novel approach investigated in this project, it is necessary to understand some fundamental aspects of localized corrosion and galvanic corrosion.

As described above, SS exhibits corrosion resistance because of the presence of a thin Cr-rich oxy-hydroxide film, the so-called passive film that forms spontaneously on the surface. However, SS, like other passive metals, is susceptible to localized corrosion in aggressive chloride-containing environments. Localized corrosion in the form of pits and crevices will initiate above a characteristic breakdown potential in a given environment. Localized corrosion will tend not to initiate below this potential, and one design criterion for preventing localized corrosion is to require that the corrosion potential stay lower than the breakdown potential. However, localized corrosion can propagate at potentials lower than the breakdown potential, but not below a characteristic repassivation potential. Therefore, a more conservative design criterion is that the corrosion potential must stay below the repassivation potential.

When two different metals are electrically coupled (as are a weld and base metal) and exposed to the same environment, galvanic interactions will occur. The more active metal (or less-noble metal, i.e. the one with the lower corrosion potential in that environment) will undergo accelerated attack and the more noble metal will be protected. This galvanic protection is a form of cathodic protection and is the mechanism explaining how a steel substrate is protected from corrosion by Zn coating in a galvanized structure. Sacrificial protection of steel hulls by Mg anodes is now old technology.

One key aspect in galvanic coupling is the area ratio of the two metals. It can be shown that  $i_a$ , the anodic current density or corrosion rate of the anode or less noble metal, depends upon the ratio of the areas of the cathode and anode,  $A_c$  and  $A_a$ , and the current density at the cathode,  $i_c$ , according to:

$$i_a = \frac{A_c}{A_a} i_c \quad (1)$$

The galvanic potential will also depend upon the area ratios. If one area is significantly larger than the other, then the galvanic potential of the couple is pinned at the uncoupled corrosion potential of the larger metal. For a welded stainless steel structure, the area of the weld metal is much less than the area of the substrate being welded, which means that the potential of the weld will be set by the corrosion potential of the stainless steel in the particular environment. If the weld metal is less noble than the stainless steel, the galvanic coupling will result in an increase in the potential of the weld. This can result in aggressive attack of the weld if the stainless steel corrosion potential is above the breakdown potential of the weld, or if the less noble weld metal does not passivate and dissolves actively. However, if the weld metal is noble relative to the stainless steel, then the galvanic coupling will result in cathodic protection of the weld metal by the stainless steel. This is the basis of the novel concept in this project.

In summary then, a new weld metal for SS must meet the following design criteria:

3. The breakdown and repassivation potentials of the weld metal should be higher than the corrosion potential of the SS substrate to prevent localized attack of the weld metal.
4. If possible, the corrosion potential of the weld metal should be slightly higher than that of the SS substrate so that the weld metal is cathodically protected.

## **9. Materials and Methods**

Guidance on galvanic interactions can be obtained by the galvanic series. The open circuit potential (OCP) of Monel-400 is in the similar range as those of the austenitic stainless steels in seawater, distilled water, potable water, HCl, and H<sub>2</sub>SO<sub>4</sub>. Alloy 400, commonly known as Monel contains 31% Cu (typical value), and maximum concentrations in wt% of 2.5% Fe, 2% Mn, 0.5% Si, 0.3% C, and 0.024 % S. Monel has good corrosion, erosion and cavitation resistance in seawater and is widely used in seawater under conditions of high flow velocity such as propellers, shafts, condenser tubes and heat exchangers. Also, Ni-Cu alloys reportedly form shallow rather than deeply penetrating pits in chloride environments during long-term exposure tests. Therefore, Monel was chosen as the starting point for this study.

Welds were fabricated in 304L stainless steel plate using Gas Tungsten Arc Welding (GTAW). Details of the welding process are given below. The welds were characterized by optical and electron microscopies, microhardness profiling, bend testing and transverse tensile testing.

A large number (more than 200) of Ni-based alloy buttons were fabricated by electric arc melting. The alloying elements, including Cu, Pd, Mo, Fe, and Cr, were varied over a wide range. Details are given below. The buttons were tested in the as-cast and solutionized conditions. Buttons and weld samples were immersed in artificial seawater and 0.1 M NaCl for extended periods. During these long term exposure tests, the corrosion potentials and polarization resistance values of the samples were measured. Other electrochemical tests include potentiodynamic polarization and galvanostatic testing.

## 10. Results and Accomplishments

Detailed results of this project can be found in three publications that are attached in the appendix of this report. This section will summarize the findings in an abbreviated manner. Interested readers are referred to the papers in the appendix for the detailed descriptions.

Welds were made in 304L plate stock using commercial 308L or Monel (AWS ERCuNi) consumables. Only recently have we been able to obtain weld wire fabricated from our “optimized” composition, and welding with that wire is just underway. Most of the welds were made using the GTAW process. Considerable process development was required to arrive at the GTAW process conditions that resulted in high quality welds. It was necessary to limit the heat input and to shield with Ar- 5% H<sub>2</sub> gas, since high heat input welds exhibited cracking and pure Ar shielding led to slagging. Table 1 shows the welding process details.

Table 1. Details of GTAW procedure

Current	150 Amp
Voltage	12 V
Travel speed	5 in/min
Heat input	21.6 kJ/in (0.85 kJ/mm)
Wire feed speed	45 in/min
Shielding gas	Argon + 5% H <sub>2</sub>
Shielding gas flow rate	30 ft <sup>3</sup> /min
Joint design	V- groove 90°, gap: 0.118 in

Figure 1 shows a high quality 304L/Monel weld. Welds such as these passed bend tests using a 1.9 cm diameter mandrel and exhibited mechanical properties, such as hardness, strength and ductility that are similar to those obtained from 304L/308 welds. The weld metal was found to be fully austenitic with perhaps some second phase formation in the interdendritic regions. Details of the metallographic analysis are found in the appended papers.



Figure 1. High quality Monel/304L weld.

Long Term Exposure (LTE) tests were carried out in artificial seawater for up to 50 days. Figure 2 shows a 304L/Monel sample after 50 days exposure. As seen in this figure, the weld top surface was not heavily attacked. However, the bottom surface of the weld exhibited pits and intergranular corrosion in the weld metal near the interface, Figure 3

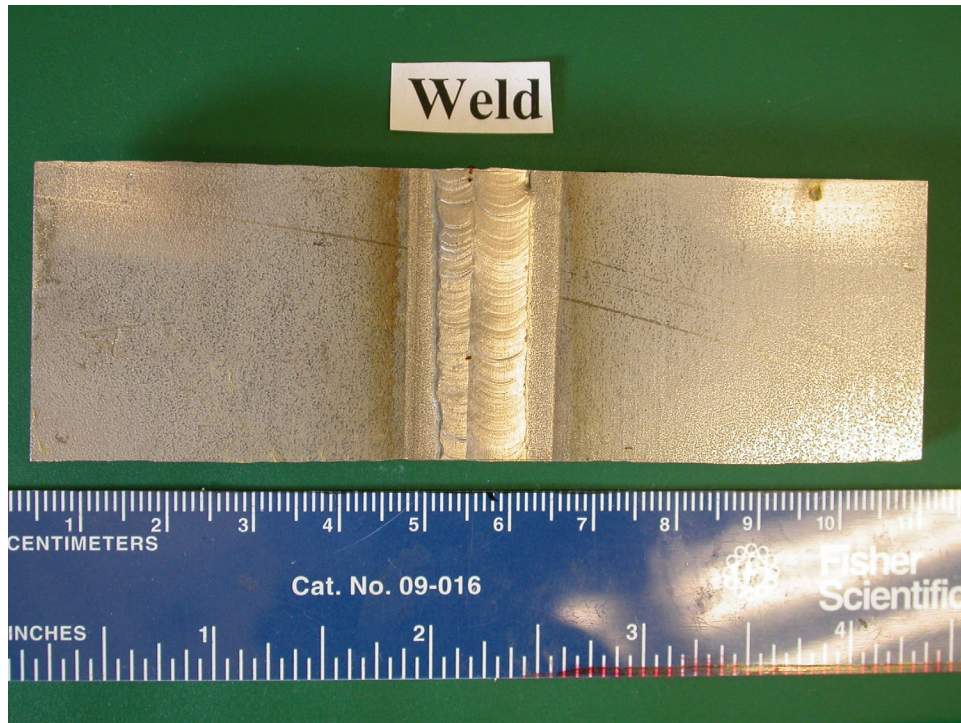


Figure 2. 304L/Monel weld after 50 days exposure in aerated artificial seawater.

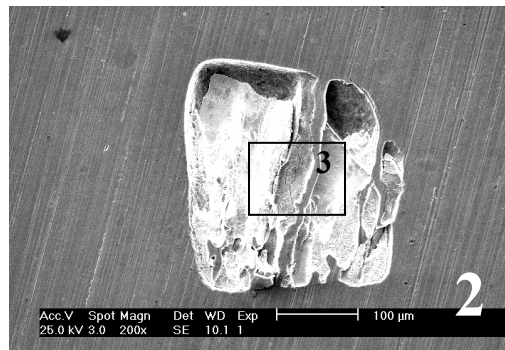


Figure 3. Example of pit formed in 304L/Monel weld after 50 days exposure in artificial seawater.

The 304L/Monel weld retained its passivity during LTE tests in 0.1 M NaCl, with no evidence of localized corrosion. However, purposeful polarization to high potentials resulted in attack at the Cu-rich interdendritic region in the weld microstructure. Figure 4 summarizes the breakdown potentials and open circuit potentials (OCPs) observed after 14 days in 0.1 M NaCl. For all

materials studied, the OCP was below the breakdown potential, indicating stable passivity. Furthermore, the OCP of 304L was below the breakdown potential of the weld.

Because the welds break down at Cu-rich segregated regions, it is of interest to understand better the effects of Cu on the corrosion properties. Figure 5 shows the results of potentiodynamic polarization measurements that were made on polished samples in artificial seawater. The corrosion potential in aerated artificial seawater was found to increase with increasing Cu content of the binary alloys. Monel 400 had a similar corrosion potential as Ni-30Cu. The breakdown potentials measured in both aerated and deaerated artificial seawater decreased with increasing Cu content for the binary alloys. Monel K400 exhibited lower breakdown potentials than Ni-30Cu and the Monel/304L weld exhibited similar breakdown potentials as Ni-45Cu. The breakdown potential of stainless steel 304L was the highest.

To investigate the effect of the segregation on the corrosion properties in Ni-Cu alloys, two welds having different level of dilution were annealed at 1150°C for 1 h to homogenize the microstructure and then rapidly cooled. After annealing, the breakdown potentials of the two welds were increased by 50 - 80 mV. The fact that homogenization improved the breakdown behavior of the Monel/304L welds further supports the notion that micro-segregation of Cu dominates the corrosion resistance of Ni-Cu welds.

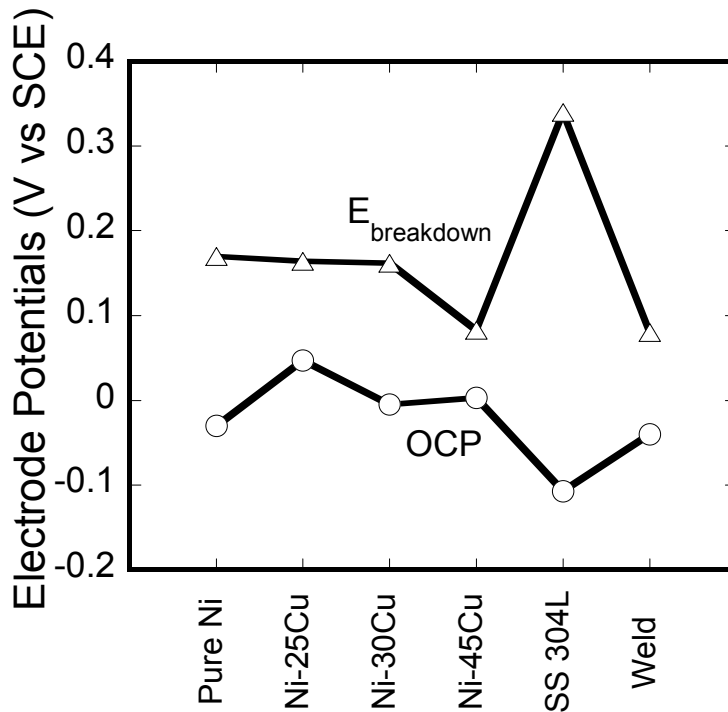
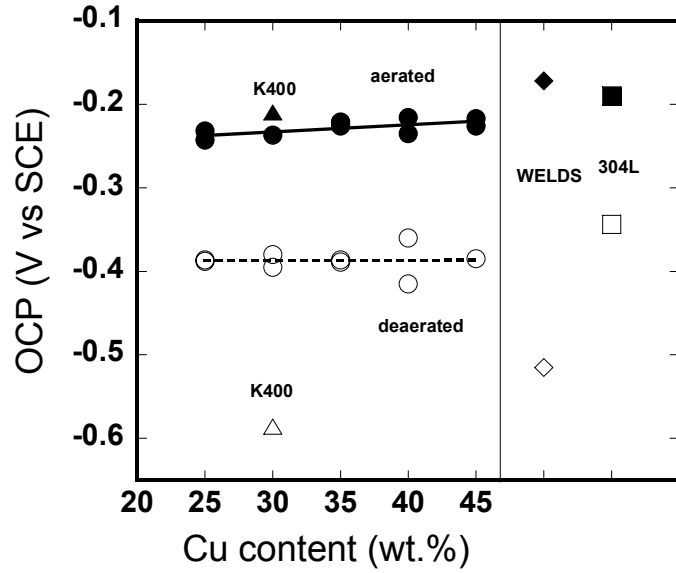
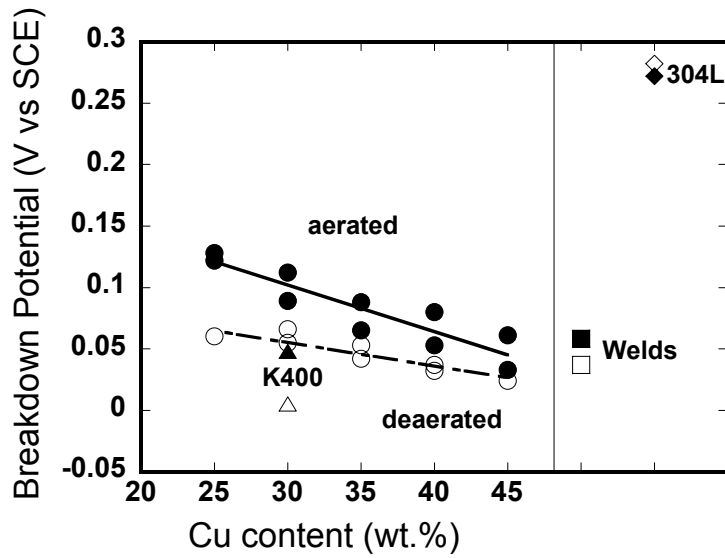


Figure 4. Summary of breakdown and open circuit potentials (OCP) for 304L/Monel weld and a number of other materials in 0.1 M NaCl at the end of 14 days exposure.



a)



b)

Figure 5. Effect of Cu content on results from potentiodynamic polarization curves for Ni-Cu alloys and weld in artificial seawater. open symbols – deaerated, closed symbols – aerated. a) open circuit corrosion potential b) breakdown potential.

Work was performed on a series of samples prepared by arc-melting to investigate the role of alloying on the corrosion properties. The first set of experiments focused on alloys with Ni:Cu ratio of 7:3, similar to that of Monel. These samples were cast, rolled, solutionized at 1100°C for 1 h and then either water quenched or furnace cooled. The results of these experiments supported the conclusions drawn above, that Cu contents lower than Monel concentrations should be investigated. The effects of small Pd or Mo additions, as well as combined additions of Pd and Mo were studied. Pd had a large beneficial effect, Figure 6, but Mo additions were detrimental, and no synergism between Pd and Mo was observed. The influences of Fe and Cr additions separately, as well as together, were studied as a means of addressing the effects of dilution of the weld metal by base metal. Dilution of Ni-Cu with stainless steel up to 15% improved the localized corrosion resistance, but slightly decreased the corrosion potential, Figure 7. Further dilution degraded the corrosion resistance.

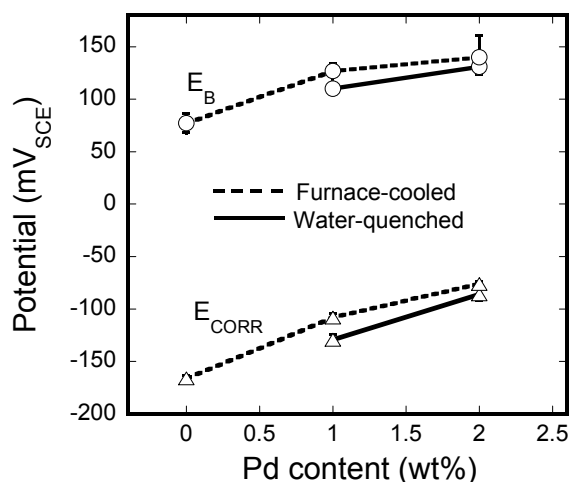


Figure 6. The effect of Pd content on the  $E_{CORR}$  and  $E_B$  of furnace-cooled and water-quenched 7:3 Ni-Cu alloys in aerated 0.1 M NaCl.

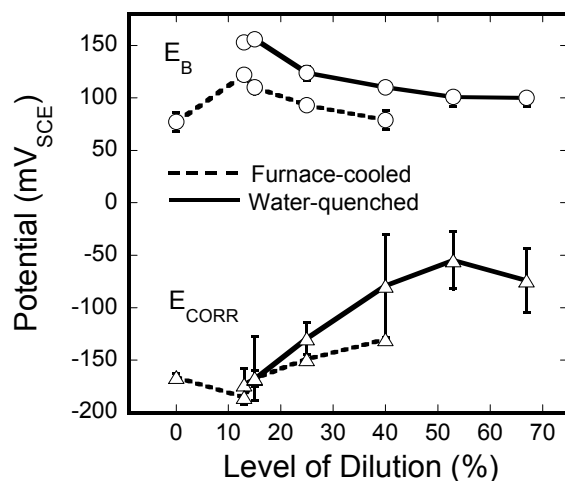


Figure 7. The effect of dilution on the  $E_{CORR}$  and  $E_B$  of furnace-cooled and water-quenched 7:3 Ni-Cu alloys in aerated 0.1 M NaCl.

Another series of experiments was performed on electric-arc melted buttons that were tested in the as-cast state to simulate the as-welded microstructure. Lower concentrations of Cu and the effects of dilution were investigated, Figure 8. Ni-Cu alloys with 5-10 wt% Cu had the highest breakdown and repassivation potentials. The addition of 5% Cu was sufficient to increase the corrosion potential above that of pure Ni, but little benefit was obtained with more Cu. As a result, further work was focused on Ni with 5 or 10 wt% Cu. Alloys with 5 or 10 wt% Cu and small amounts of Pd, Mo, or both Pd and Mo were fabricated. The behavior was identical for alloys with the same amount of Pd and Mo, but either 5 or 10 wt% Cu. Figure 9 shows the corrosion, breakdown, and repassivation potentials for Ni-10Cu alloys containing Pd, Mo, or both Pd and Mo. The effects of 25 and 50% dilution on these alloys are also shown. The values of  $E_B$ ,  $E_{CORR}$ , and  $E_{RP}$  for almost every level of dilution were highest for the alloy with 1 wt% Pd.  $E_{CORR}$  and  $E_{RP}$  for the 1 wt% Pd were higher than those of type 304L stainless steel for all dilution levels, but  $E_B$  was still lower by 70-80 mV. Mo addition of 3 wt% was only beneficial at the very high dilution of 50%, but it exhibited the lowest  $E_{RP}$  and  $E_{CORR}$  at almost all dilution levels. The addition of both Mo and Pd resulted in values between those for the Ni-Cu alloys alloyed with only Pd and only Mo.

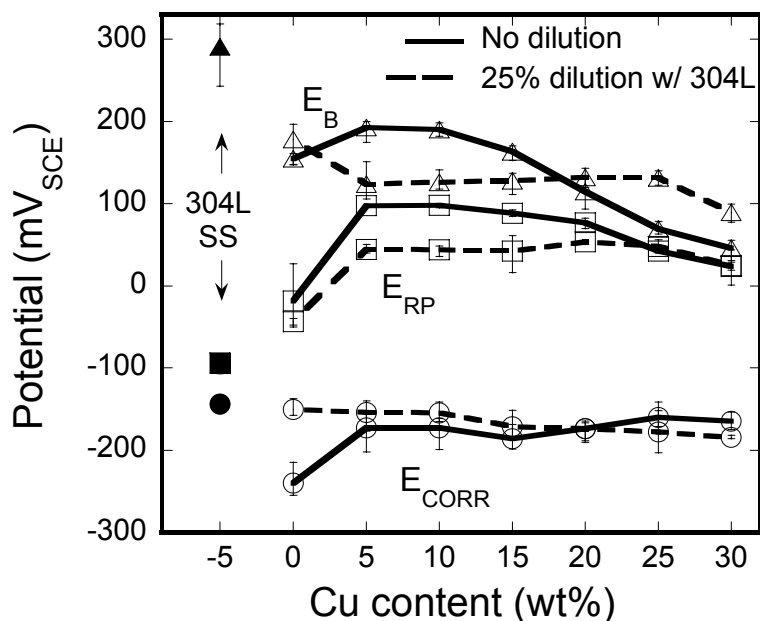
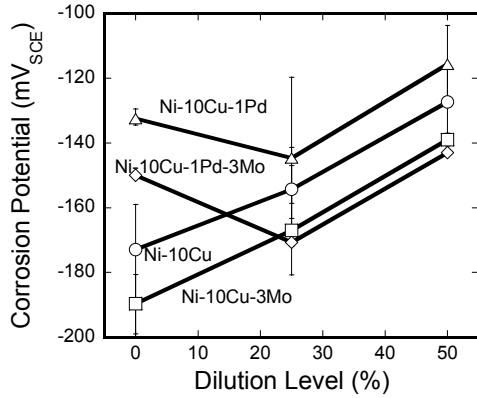
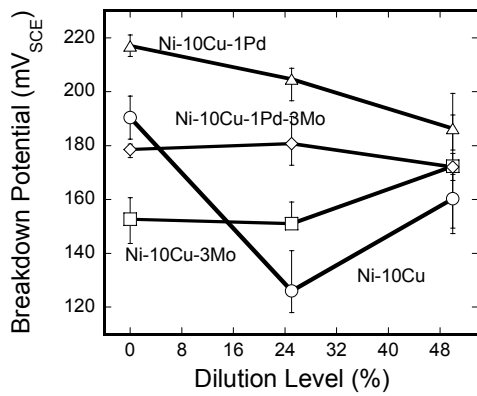


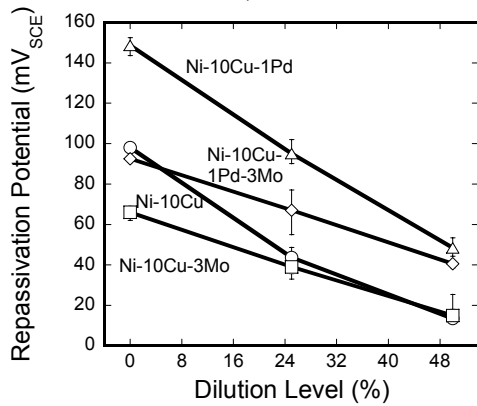
Figure 8. The effect of Cu content on the  $E_{CORR}$ ,  $E_B$ , and  $E_{RP}$  of as-cast Ni-Cu alloys with and without 25% dilution in aerated 0.1M NaCl. The values for type 304L stainless steel are shown at left of plot for comparison.



a)



b)



c)

Figure 9. The effect of alloying elements of Pd and Mo on the  $E_{CORR}$  (a),  $E_B$  (b), and  $E_{RP}$  (c) of as-cast Ni-10Cu alloys with the dilution of 0%, 25% and 50% in aerated 0.1 M NaCl.

The alloy Ni-(5-10)Cu-1Pd meets the design criteria for a Cr-free welding consumable for 304L stainless steel; it has a breakdown potential above the corrosion potential of type 304L SS and a corrosion potential slightly above that of type 304L SS. Furthermore, it has the highest breakdown and repassivation potentials of the alloys studied, and a repassivation potential that is significantly higher than that of type 304L stainless steel. These relationships are clearly seen in

Figure 10, which is a comparison of representative cyclic polarization curves for the optimized alloy Ni-10Cu-1Pd alloy, Monel K-400, type 304L stainless steel, and a conventional 304L/308L weld in aerated 0.1 M NaCl. The NiCuPd alloy exhibits an increase in the passive current density at around 70 mV SCE, but the same  $E_B$  as the 304L/308L weld according to the definition of breakdown potential used in this study. This value of  $E_B$  is about 100 mV below the value for 304L. Furthermore, the  $E_{RP}$  for the alloy is seen to be much higher than the values for 304L or the 304L/308L weld.

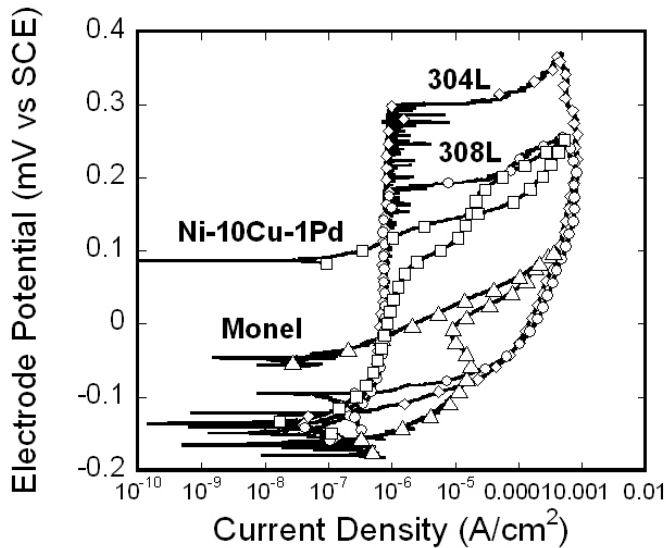


Figure 10. Cyclic polarization behavior of type 304L stainless steel, conventional weld of 308L, as-cast Ni-10Cu-1Pd alloy, and Monel in aerated 0.1 M NaCl.

Preliminary fume analysis studies were performed to validate that the use of Cr-free consumables will in fact reduce the Cr content of welding fumes. Type 304L SS plate was welded using an SMAW process with either standard 308L welding rod or the Monel weld rod. The weld fumes were collected, separated into 3 different sizes with a particle impactor, and examined in an SEM with EDS. EDS does not differentiate oxidation state; only total Cr content was determined. The Cr content of the welding fume for a 19% dilution weld made with a Monel weld rod was  $0.24 \pm 0.12$  wt% Cr, and for a standard weld made with a 308L weld rod it was  $3.5 \pm 1.3$  wt% Cr. So the improvement was more than a factor of 10. The emission was not zero because Cr from the base metal was diluted into the weld and a portion was entrained in the weld fume. However, this proves that the consumable is the major source of Cr (308L contains 19.5-22 %Cr) and that the emission of Cr is reduced by removing Cr from the consumable.

## 11. Conclusions

High quality welds in 304L SS have been produced with no cracks. The welds pass bend tests and exhibit mechanical properties that are comparable to welds made with standard 308L SS consumables. The 304L/Ni-Cu welds have survived exposure tests in mildly aggressive environments such as immersion in aerated 0.1 M NaCl for 2 weeks with no evidence of attack. A large amount of electrochemical data has been collected to support these observations.

The parameters studied to date include the effects of Cu content over a certain range, small levels of Pd or Mo additions, dilution by 304L base metal, and solution flow. Preliminary examination and characterization of the weld microstructure has been completed.

Ni-Cu alloys containing other minor alloying element additions were studied in aerated 0.1 M NaCl to develop a material with suitable corrosion properties for use as a Cr-free consumable for welding type 304L stainless steel. The addition of 5~10wt% Cu to Ni improved the resistance to localized corrosion. Pd additions in the range of 1-2% had a large influence in ennobling the  $E_{CORR}$  and improving the localized corrosion behavior of Ni-Cu alloys. The addition of Mo was not effective for improving the breakdown behavior of Ni-Cu alloys. The addition of up to 10 wt% Fe improved the breakdown behavior of Ni-Cu, but larger amounts of Fe decreased  $E_B$ . Slow-cooling of Ni-Cu alloys containing Fe degraded the localized corrosion resistance. Cr addition increased  $E_B$  but slightly decreased  $E_{CORR}$ . The addition of more than 3 wt% Cr did not further improve the breakdown behavior, but slow-cooling degraded the localized corrosion resistance. Dilution of Ni-Cu with stainless steel up to 15% improved the localized corrosion resistance, but slightly decreased  $E_{CORR}$ . Further dilution degraded the corrosion resistance. Low heat input and fast cooling rate should minimize the deleterious segregation and dilution effects on the corrosion properties of a weld made with a Ni-Cu consumable.

The optimized composition for a new Cr-free consumable for welding type 304 stainless steel is Ni-(5~10)Cu-1Pd.  $E_{CORR}$  of this alloy in 0.1M NaCl was slightly higher than that of type 304L stainless steel. The  $E_B$  of this alloy was slightly lower than that of conventional weld made with 308L filler metal, but its  $E_{RP}$  was much higher.

## 12. Appendices

Appended to this document are copies of three publications that were developed from this work:

1. J.C. Lippold, G. Guaytima, G.S. Frankel, and Y.H. Kim, "Development of Ni-Cu Filler Metals for Joining Austenitic Stainless Steels," *Stainless Steel World 2004*, KCI Publishing BV, Zutphen, The Netherlands, pp. 140-148.
2. Yeong Ho Kim, G. S. Frankel, J. C. Lippold and G. Guaytima, "Cr-free Consumables for Welding Stainless Steel. Part 1: Monel," submitted to *Corrosion* for publication, 12/2004.
3. Yeong Ho Kim, G. S. Frankel, J. C. Lippold and G. Guaytima, "Cr-free Consumables for Welding Stainless Steel. Part 2: Optimization of Alloy Composition Based on Corrosion Behavior", submitted to *Corrosion* for publication, 12/2004.

# Development of Ni-Cu Filler Metals for Joining Austenitic Stainless Steels

J.C. Lippold, G. Guaytima, G.S. Frankel, and Y.H. Kim, The Ohio State University

Keywords: Stainless steel, Monel, Ni-Cu alloys, welding, corrosion, mechanical properties, welding fume

## Abstract

Consumables for austenitic stainless steels normally contain chromium levels that match or exceed the level of the base metal. During arc welding, evaporation and oxidation from the molten weld pool results in the generation of various compounds and metallic species in the welding fume, including compounds containing carcinogenic hexavalent Cr ( $\text{Cr}^{+6}$ ). Significant quantities of  $\text{Cr}^{+6}$  can form, resulting in a health hazard for the welder. In this investigation, Ni-Cu alloys with some minor alloying additions have been developed as potential replacements for standard austenitic stainless steel filler metals.

ERNiCu-7 (Monel™ 60) filler metal was used to perform gas tungsten arc welds in Type 304L base metal. Under optimized conditions, high quality welds were produced that exhibited mechanical properties comparable to 308L/304L welds. Additional work has been conducted to investigate Ni-Cu alloys that have good corrosion resistance when used to weld Type 304L. This has resulted in the development of Ni-Cu alloys containing additions of palladium. The corrosion resistance of these alloys has also been evaluated in mildly aggressive environments, such as immersion in aerated 0.1 M NaCl for 2 weeks, with no evidence of attack. This paper will describe details of the welding metallurgy and corrosion studies that have been conducted.

## Introduction

Consumables for austenitic stainless steels normally contain chromium levels that match or exceed the level of the base metal.<sup>1</sup> During arc welding, evaporation and oxidation from the molten weld pool results in the generation of various compounds and metallic species in the welding fume, including compounds containing carcinogenic hexavalent Cr ( $\text{Cr}^{+6}$ ). Significant quantities of  $\text{Cr}^{+6}$  can form, resulting in a health hazard for the welder.<sup>2</sup> The Permissible Exposure Limit (PEL) for  $\text{Cr}^{+6}$  exposure is currently under review by OSHA, and a significantly lower PEL could be put into effect within a few years. New regulations might restrict the welding of stainless steel in environments that are difficult to ventilate, such as ship interiors. It is therefore of interest to develop materials and processes to weld stainless steel with decreased  $\text{Cr}^{+6}$  emission.

It is possible to eliminate fume generation by utilizing a solid state welding process such as friction welding or friction stir welding. These processes require complete re-engineering of the welding process and are limited in terms of their application. It is the goal of this investigation to develop a Cr-free filler metal that would be a drop-in replacement for conventional welding consumables for austenitic stainless steels.

Corrosion resistance is the absolute key to developing a successful approach to welding austenitic stainless steel with Cr-free consumables, since these materials are normally used in corrosive environments. If the welds are susceptible to corrosion, then the liabilities from the fabrication process will negate the benefits of stainless steel.

Stainless steel obtains its corrosion resistance from the addition of Cr; steel becomes stainless when it contains greater than about 12% Cr.<sup>3</sup> The "stainless" nature is a result of the spontaneous formation of an extremely thin (a few nm in thickness) passive film that is very rich in Cr. This passive film is essentially a Cr oxy-hydroxide. The corrosion resistance of SS continues to improve with increasing Cr content, and a typical Type 304L alloy contains 18-20% Cr. Nickel is added (8-12%) to stabilize the austenite phase for improved mechanical properties.

The problem with passive metals such as stainless steels and Al alloys is that the passive film is susceptible to localized breakdown and accelerated attack, which can take the form of pits, crevices or cracks (if the material is stressed).<sup>3</sup> Localized corrosion of stainless steel typically occurs in chloride-containing environments. Improvements in localized corrosion resistance are obtained by adding 2-3% Mo to the 304L composition, increasing nickel (10-14%), and slightly reducing chromium (16-18%), resulting in a Type 316L alloy.

Because of the corrosion susceptibility associated with heat-affected zones and with segregation and second phase formation in the fusion zone, welds are usually the sites of corrosion attack in welded structures.<sup>4</sup> Therefore, it is common to use weld filler metal that is higher in Cr than the base metal. For example, Type 304L with 18-20% Cr is typically welded with a Type 308L consumable with 19-22% Cr. Weld filler metals with higher Cr levels increase the generation of hexavalent Cr in the welding fume.

Selection of a Cr-free consumable requires consideration of galvanic interactions with the austenitic stainless steel base metal. Guidance on galvanic interactions can be obtained by the galvanic series, which has been widely published for one environment, i.e. seawater. Figure 1 represents one form of the galvanic series.<sup>5</sup> The materials farther to the right in this figure are more noble. The ranges of potentials for 304 and 316 alloys are indicated. The materials above these alloys are graphite, Pt, Ti and several Cr rich alloys. None of these materials is suitable. However, located between the two, and almost co-located at the same potential range are the Ni-Cu alloys 400 and K-500. Alloy 400, commonly known as Monel is a very old alloy that contains 31% Cu (typical value) and maximum concentrations of 2.5% Fe, 2% Mn, 0.5% Si, 0.3% C, and 0.024 % S. Monel has good corrosion, erosion and cavitation resistance in seawater and is widely used in seawater under conditions of high flow velocity such as propellers, shafts, condenser tubes and heat exchangers.<sup>6</sup> Monel seems to form a protective oxide in neutral and alkaline solutions, which provides protection. However, it is susceptible to pitting in stagnant chloride solutions, supposedly as a result of a decrease in the supply of oxygen.

Based on this analysis, Monel was selected as a candidate Cr-free consumable. A number of issues must be considered in adopting such a consumable. From a corrosion

perspective, the corrosion potentials of the base metal and the weld metal, and the breakdown potential of the weld metal are of extreme importance. The effects of Cu content and minor alloying addition on these potentials must be considered. Also, environmental factors, such as pH, chloride concentration, aeration, temperature, and solution flow will all have an influence. From the welding point of view, the proper welding parameters to achieve a high quality weld must be determined for each combination of base metal and filler metal. The effects of welding parameters on the weld microstructure must be considered, including dilution of the filler metal by the base metal, and segregation and second phase formation. Ultimately, a weld with sufficient strength and ductility is required with no solidification cracking. Finally, the effects of weld metal composition and welding parameters on welding fume composition must be understood.

## Experimental Procedure

Welds were produced in 0.25-in. (6.4 mm) thick Type 304L base metal using 0.045-in. diameter commercial Monel (AWS ERCuNi-7) and ER308L filler wire. The compositions of these materials are provided in Table 1. Also shown in Table 1 are the calculated values of weld metal composition for 15 and 40% dilution of the Monel filler metal by the 304L base metal. This represents a typical range for most arc welding processes.

Gas tungsten arc welding (GTAW) was selected to better control the dilution level. Details of the GTAW process are provided in Table 2. Shielded metal arc welding (SMAW) was used to determine fume generation rates and relative chromium concentrations. ENiCu-7 and E308-16 electrodes were used for the fume studies.

The mechanical properties of the GTA welds have been determined by tensile testing, standard face bend tests, and Vickers microhardness surveys. The weld microstructure has been characterized by optical and scanning electron microscopy (SEM). Local weld metal chemical analysis was conducted using energy dispersive spectrometry (EDS) in the SEM.

Two types of corrosion experiments have been performed. Long term exposure (LTE) tests have been performed in 0.1 M NaCl and artificial seawater. During the LTE tests, corrosion potentials and corrosion rates (by linear polarization) were measured. Potentiodynamic polarization experiments also were performed to determine the breakdown potentials.

The effect of composition on corrosion properties were determined using small, arc-melted button samples prepared from pure materials. The following ranges of alloying additions to pure nickel were evaluated: 25-45 wt% Cu, 0-10 wt% Mo, and 0-3 wt% Pd. Buttons were also prepared by mixing fixed amounts of Type 304L base metal to simulate the effect of dilution of the filler metal by the base metal.

## Results

### *Welding*

High quality GTA welds were produced using the conditions listed in Table 2. Initially, the use of 100% Ar gas for shielding resulted in a surface “slagging” effect and welds of unsatisfactory quality. This slagging was worse at high heat inputs and was related to the presence of titanium in the Monel weld wire. An example of one of these welds made at high heat input levels is shown in Figure 2. The effect was eliminated by the use of Ar-5%H<sub>2</sub> shielding gas and control of weld heat input. A weld made under the conditions listed in Table 2 is also shown in Figure 2.

Solidification cracks were observed in high-dilution welds, but not if the dilution level was kept below about 30%. A representative weld microstructure is shown in Figure 3. The weld metal was fully austenitic at dilution levels up to 40% with some evidence of interdendritic precipitation. EDS analysis showed that both Cu and Ti segregated to the interdendritic regions of the weld metal during solidification.

Transverse tensile tests were performed on Monel/304L welds at nominally 25% dilution. All failures occurred in the weld metal. The average mechanical properties were as follows: 80 ksi tensile strength, 44 ksi yield strength, and 40% elongation. These welds were also tested by bending over a ¾" mandrel, resulting in 15% tensile strain in the outer fibers. There was no evidence of cracking in any of these tests. An example of one of these samples is shown in Figure 4. The results of microhardness traverses in both Monel/304L and 308L/304L welds are shown in Figure 5. The hardness of the Monel/304L weld metal was found to be just slightly less than that of 308L/304L.

### *Corrosion*

Long term corrosion tests were performed in 0.1 M NaCl and artificial seawater open to air. No attack was observed after exposure to 0.1 M NaCl. The bottom side of the weld was attacked at the interface of the weld metal and base metal after 50 days in artificial seawater, but the top side was unattacked. Figure 6 shows the top side after the 50 day exposure.

Potentiodynamic polarization measurements were made after the LTE test in 0.1 M NaCl and the breakdown potentials were measured. The values of breakdown and corrosion potentials are given in Figure 7. As can be seen, the corrosion potential of 304L SS is below the breakdown potential of all of the materials studied, including the weld. The corrosion potential of the 304L is also slightly lower than the corrosion potentials of the other materials. As a result of the large area of the stainless steel base metal relative to the weld zone for most welded structures, these relationships result in a stable system from the galvanic corrosion perspective.

Further corrosion testing was conducted using arc-melted buttons with a range of composition. The effect of Cu content on the corrosion and breakdown potentials of simple Ni-Cu alloys, determined by potentiodynamic polarization measurements in 0.1 M

NaCl is shown in Figure 8. Since Monel is noble compared to pure Ni, it was expected that decreasing Cu content would lead to a reduction in the corrosion potential of Ni-Cu alloys, which might be deleterious to the performance of the weld. However, the Cu content had a minor effect on the corrosion potential. On the other hand, decreasing Cu had a very beneficial influence on the breakdown potential, Figure 8b.

The influence of the addition of a small amount of Pd and/or Mo was also studied as shown in Figures 9 and 10, respectively. For both alloying additions, the Cu content was held constant at 30 wt%. Pd was found to be beneficial as an alloying element in the 1-2% range. The addition of a noble metal such as Pd has been shown to provide a high exchange current density for the reduction reaction, thereby shifting the open circuit potential (OCP) higher in the passive range.<sup>7</sup> The corrosion potential and breakdown potential both increased as the Pd content increased. The effect was greater for furnace-cooled buttons compared to rapidly-cooled buttons, possibly because of segregation effects. Mo additions less than about 2% had little effect on the corrosion potential and increased the breakdown potential, which is also beneficial. However, larger additions of Mo drastically decreased the breakdown potential. There was little difference between the rapidly-cooled and furnace-cooled conditions.

The effect of dilution of Monel by an austenitic stainless steel was investigated by producing the button compositions shown in Table 3. The corrosion and breakdown potentials of these alloys are shown in Figure 11. Small levels of dilution (13 or 15%) had little influence on the corrosion potential but increased the breakdown potential. For higher dilution levels, the corrosion potential increased, but the breakdown potential decreased. Therefore, dilution levels less than 20% seem appropriate to maintain better corrosion resistance of weld metals.

Based on the corrosion studies of arc-melted buttons, and optimum composition for a Ni-Cu consumable would have lower Cu than Monel (less than 30%) and contain a few percent Pd. Dilution by the base metal must also be controlled to maintain corrosion resistance. Work is ongoing to evaluate the weldability and corrosion resistance of Ni-Cu-Pd consumables.

### ***Welding Fume Analysis***

Welding fumes were collected using an Electrical Low Pressure Impactor (ELPI) that allows fume particles to be collected according to fume particle size. In this study, fume particles in the range from 0.1 to 1.0  $\mu\text{m}$  were collected and analyzed in the SEM. Fume was collected from both E308-16 and ENiCu-7 electrodes deposited on Type 304L plate. Dilution by the Type 304L base metal in both cases was on the order of 20%.

Using SEM/EDS analysis, an average composition of the fume particles in this size range was determined. This composition is provided in Table 4. As expected, the chromium content of the ENiCu-7 fume is significantly reduced below that of the E308-16 fume (0.15 versus 3.29 wt%). Work is ongoing to determine the hexavalent Cr content of the welding fume.

## Conclusions

1. Good quality gas tungsten arc welds were achieved using ERNiCu-7 (Monel) filler metal and Type 304L base metal by controlling shielding gas and weld heat input.
2. The strength and ductility of Monel/304L GTA welds were comparable to those of 308L/304L welds.
3. Weld solidification cracking was observed at high heat inputs and dilution levels, but could be eliminated by restricting dilution below about 30%.
4. Monel/GTA welds were resistance to attack after 50 days exposure to artificial seawater.
5. Reducing Cu content and addition of Pd were found to improve the corrosion resistance of Ni-Cu alloys.

## Acknowledgments

The authors wish to acknowledge the financial support of the Strategic Environmental Research and Development Program (SERDP). Special thanks go to Mr. Jeff Sowards of the Welding Engineering Program at OSU who assisted with the weld fume collection.

## References

1. ASM Handbook, 10th Edition, Volume 6, Welding, Brazing, and Soldering, ASM International, 1993.
2. AWS, 1995. "Chromium and Nickel in Welding Fume", Safety and Health Fact Sheet No. 4. Second Edition.
3. A.J. Sedriks, Corrosion of Stainless Steels, 1996, Wiley-Interscience, NY.
4. T.G. Gooch, 1996. Corrosion Behavior of Welded Stainless Steel, *Welding Journal*, 75(5):135s.
5. A.H. Tuthill and C.M. Schillmoller, 1971. *Guidelines for Selection of Marine Materials*, International Nickel Company.
6. Special-Metals, "Technical Bulletin Monel Alloy 400", <http://www.specialmetals.com/products/monelalloy60.htm>.
7. J. H. Potgieter, 1991. *Journal of the Applied Electrochemistry* **21**, 471-482.

Table 1. Composition of filler metals and base metal. Calculated weld metal composition for 304L/Monel welds at 2 different dilutions are also provided.

<b>Element (wt%)</b>	<b>Monel</b>	<b>304L SS</b>	<b>308L SS</b>	<b>15% Dilution calculated</b>	<b>40% Dilution calculated</b>
Ni	63.99	8.08	9-11	55.60	41.63
Cu	28.81	-	0.75 max	24.49	17.29
Fe	0.76	72.10	65	11.46	29.30
Cr	-	18.09	19.5-22.0	2.71	7.24
Mn	3.49	1.24	1.0-2.5	3.15	2.59
Ti	1.99	-		1.69	1.19
Si	0.90	0.37	0.3-0.65	0.82	0.69
N	-	0.06		0.01	0.02
C	0.05	0.03	.08 max	0.05	0.04
Others	0.01	0.03		0.01	0.02

Table 2. Details of Gas Tungsten Arc Welding Procedure

Current	150 Amp
Voltage	12 V
Travel speed	5 in/min
Heat input	21.6 kJ/in (0.85 kJ/mm)
Wire feed speed	45 in/min
Shielding gas	Argon + 5% H <sub>2</sub>
Shielding gas flow rate	30 ft <sup>3</sup> /min
Joint design	Double V- groove 90°, gap: 0.118 in

Table 3. Composition of Arc-Melted Buttons for Determining the Effect of Dilution of a 70Ni-30Cu alloy by Fe and Cr

Alloy	Button Composition, wt%				Dilution, %
	Ni	Cu	Fe	Cr	
D0	61	26	10	3	13
D1	59.5	25.5	10	5	15
D2	52.5	22.5	20	5	25
D3	42	18	30	10	40
D4	33	14	40	13	53
D5	23	10	50	17	67

Table 4. Composition of Welding Fume determined using SEM/EDS.

Electrode	Composition(wt%)						
	Fe	Cr	Ni	Cu	Mn	Si	Ti
ENiCu-7	-	0.15	3.1	8.1	2.5	0.8	-
E308-16	1.8	3.29	-	-	1.6	8.0	0.01
	Composition (wt%)						
	C	O	F	Na	Al	Ca	K
ENiCu-7	-	12.3	26.9	26.0	14.2	1.89	1.71
E308-16	9.0	25.2	17.1	3.4	-	-	22.6

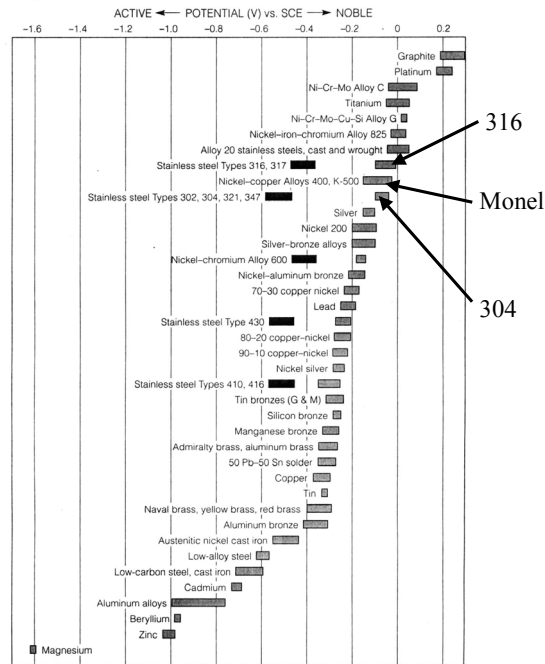


Figure 1. The galvanic series in seawater. Note that the potential for Monel overlaps that of Type 304 stainless steel. (Ref. 5)

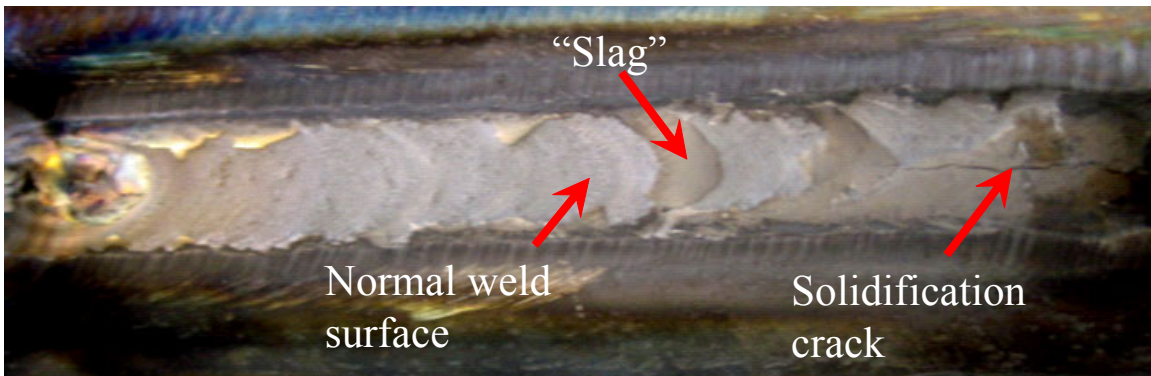


Figure 2. Monel/304L welds made using GTAW. High heat input welds with argon shielding gas exhibited surface “slagging” and solidification cracking (above). The use of 95Ar-5H<sub>2</sub> shielding gas produced good quality welds (left).

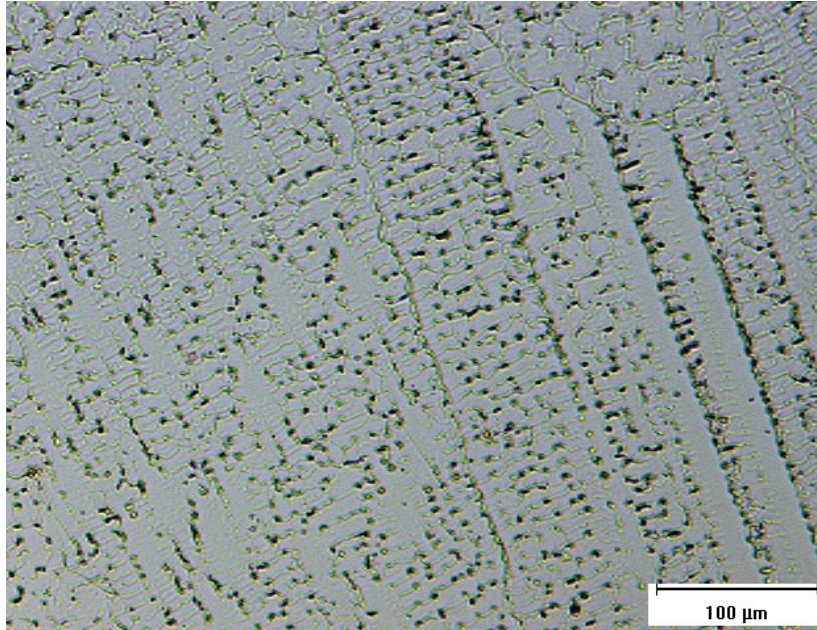


Figure 3. Representative weld metal microstructure of Monel/Type304L GTA welds.



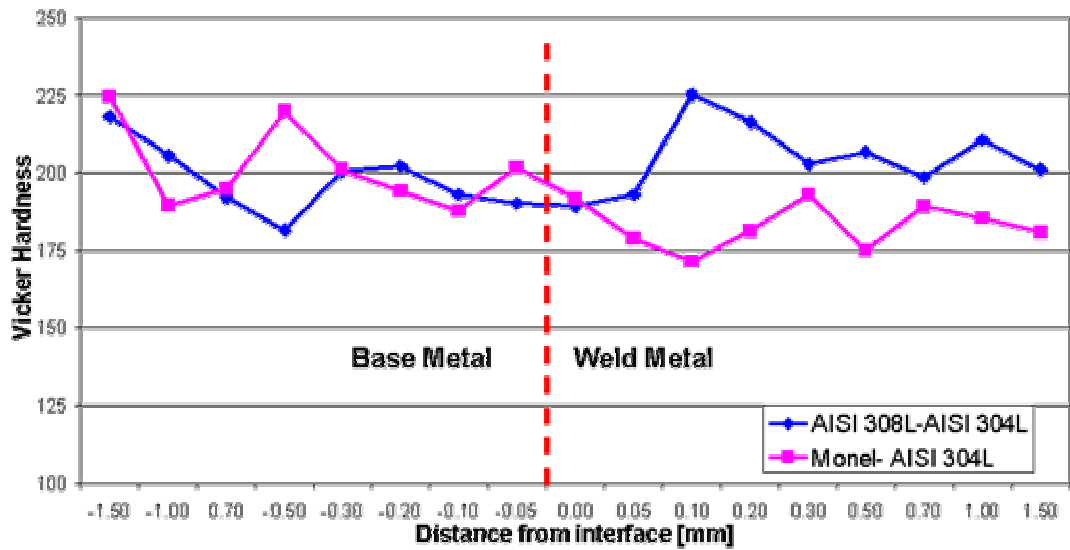
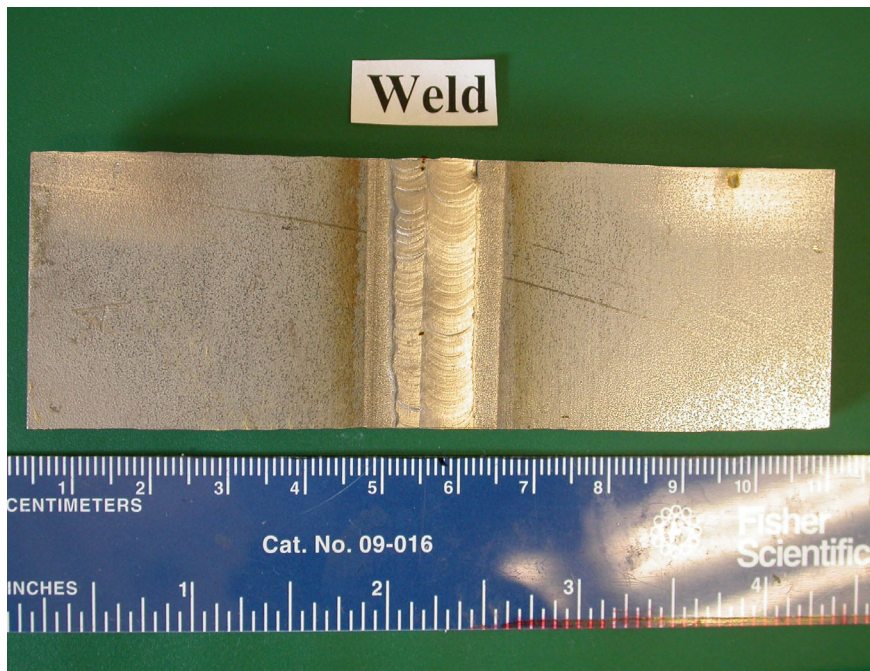


Figure 5. Microhardness traverses from the base metal (left) into the weld metal of Monel/304L and 308L/304L GTA welds.



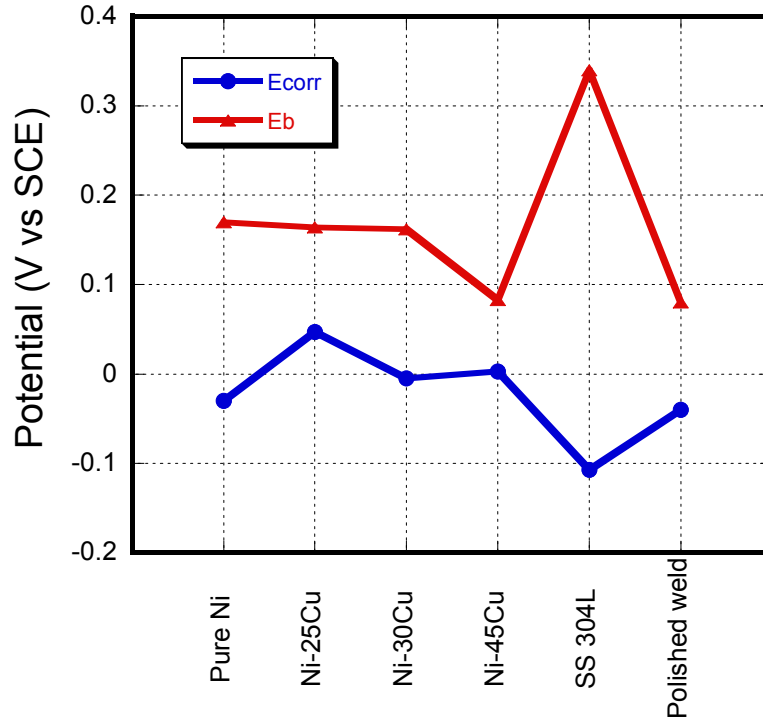


Figure 7. Corrosion potentials and breakdown potentials for different metals after 14 days immersion in 0.1 M NaCl.

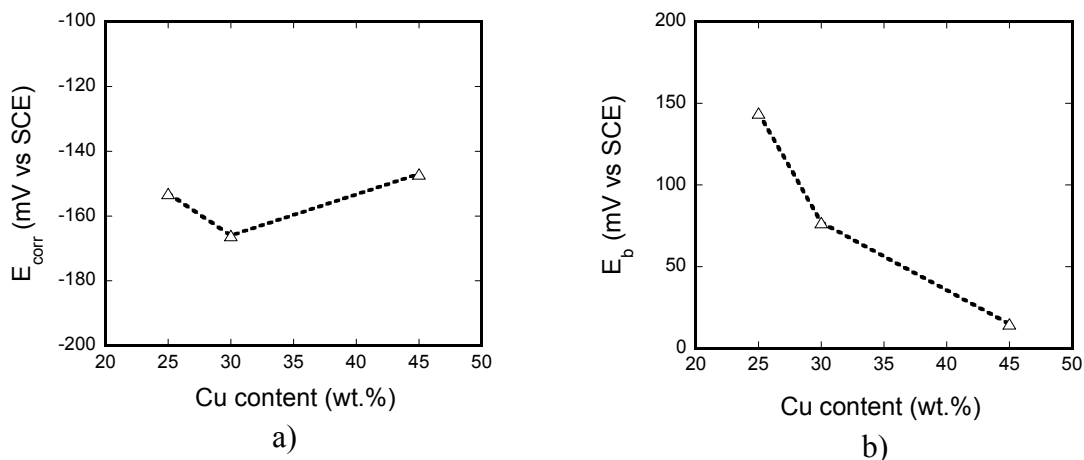


Figure 8. The effect of Cu content in binary Ni-Cu alloys on a) corrosion potential and b) breakdown potential in 0.1 M NaCl.

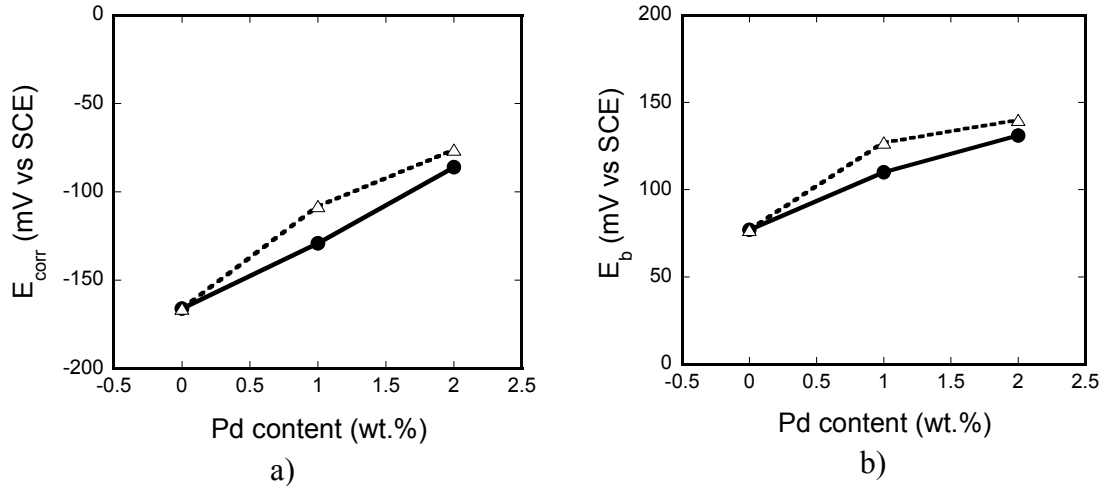


Figure 9. The effect of Pd content in Ni-30Cu alloys on a) corrosion potential and b) breakdown potential in 0.1 M NaCl. Filled symbols = rapidly cooled, open symbols = furnace cooled.

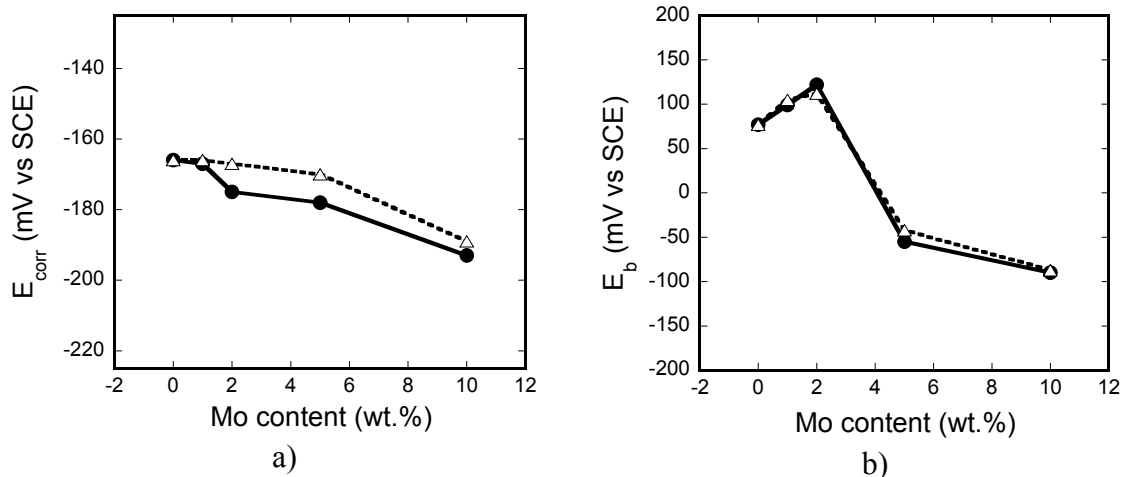


Figure 10. The effect of Mo content in Ni-30Cu alloys on a) corrosion potential and b) breakdown potential in 0.1 M NaCl. Filled symbols = rapidly cooled, open symbols = furnace cooled.

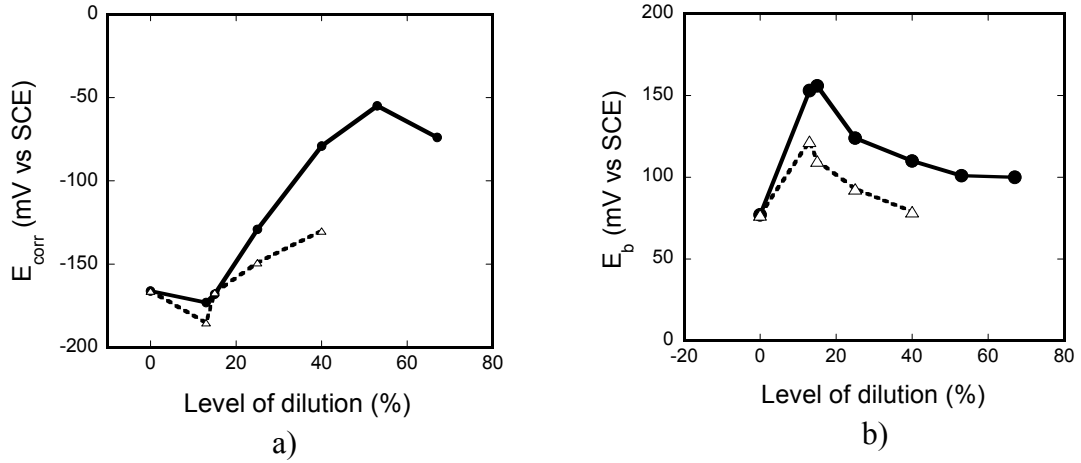


Figure 11. The effect of level of dilution of 70Ni-30Cu alloys by Fe and Cr on a) corrosion potential and b) breakdown potential in 0.1 M NaCl. Filled symbols = rapidly cooled, open symbols = furnace cooled.

## **Cr-free Consumables for Welding Stainless Steel. Part 1: Monel**

Yeong Ho Kim\*, G. S. Frankel\*, J. C. Lippold\*\* and, G. Guaytima\*\*

\*Fontana Corrosion Center, Dept. of Materials Science and Engineering

\*\*Dept. of Industrial, Welding, and Systems Engineering

The Ohio State University

Columbus, OH 43210

### **Abstract**

During fusion welding of stainless steels and other high-Cr alloys, evaporation and oxidation of Cr from the molten weld pool result in the generation of carcinogenic hexavalent chromium (Cr(VI)) in the welding fume. Stringent new exposure limits from OSHA might limit the environment in which welding of stainless steel will be possible in the future. Therefore, a Cr-free filler metal is needed to reduce the release of Cr(VI) during welding of stainless steel. From the galvanic series, the corrosion potential of the Ni-Cu alloy K400 is located in the same potential range as types 304 and 316 stainless steels. In this study, the applicability of the Monel-type filler metals for the welding of austenitic stainless steel is examined. Type 304L stainless steel plate was successfully welded with Monel filler wire, resulting in high quality welds with no cracks. The welds survived long term exposure to mildly aggressive environments like 0.1 M NaCl with no evidence of corrosion. However, Cu-rich regions in weld were the weak spots for corrosion susceptibility.

Keywords: Welding, stainless steel, Monel, galvanic corrosion

Contact info: GS Frankel, 477 Watts Hall, 2041 College Rd. Columbus, OH 43210 tel: 614-688-4128, fax 614-292-9857, [frankel.10@osu.edu](mailto:frankel.10@osu.edu) (until June: Max Planck Institute fur Eisenforschung, Max-Planck-Str. 1, D-40237, Duesseldorf, Germany)

### **Introduction**

There is a wide range of welding processes, most of which involve the formation of a molten metal zone. The very high temperatures in the weld pool result in considerable vaporization of metal and generation of a fume that contains fine particles of metal in various oxidation states<sup>1,2,3</sup>. In many cases, weld fumes are an extreme danger to the health of the welder<sup>1,4</sup>. For welding of stainless steel, of particular interest is the Cr(VI) content (Cr (VI) is chromium in the 6<sup>+</sup> oxidation state and is commonly referred to as chromate). Fumes containing Cr(VI) can cause lung cancer.<sup>1,4</sup> In shipbuilding operations, manual Shielded Metal Arc Welding (SMAW) of stainless steel is often performed in cramped conditions, such as within the interior of a ship, where ventilation to remove the dangerous fumes is difficult. The problem will become more severe if the Permissible Exposure Limit (PEL) for Cr(VI) set by the Occupational Safety and Health Administration (OSHA) is lowered<sup>5</sup>. The major source of material for a weld fume is the consumable, although base metal diluted into the weld can also end up in the fume. Clearly it is of interest to limit the generation of dangerous fumes by decreasing the content in the consumable of metals such as Cr and Mn that are unhealthy when present in fumes.

The objective of this study is to develop a Cr-free consumable and a process for welding stainless steel. From a welding perspective, solidification cracking, intermediate temperature embrittlement, and alloy hot formability need to be understood. The critical corrosion issues include the susceptibility to localized corrosion, dealloying effects during long term exposure, solution flow effects, and environmental cracking.

If stainless steel is to be welded with a filler metal that is different in composition than the base metal, then the corrosion of the welded structure will be controlled by the phenomena of galvanic corrosion<sup>6,7,8</sup> and localized corrosion. Localized corrosion in the form of pits and crevices will initiate above a characteristic breakdown potential in a given environment, and one design criterion for preventing localized corrosion is to require that the corrosion potential stay lower than the breakdown potential. However, localized corrosion can propagate at potentials lower than the breakdown potential, but not below a characteristic repassivation potential. Therefore, a more conservative design criterion is that the corrosion potential must stay below the repassivation potential.

One key aspect in galvanic coupling is the area ratio of the two metals, which determines the galvanic potential<sup>9,10,11,12</sup>. If one area is significantly larger than the other, then the galvanic potential of the couple is usually equal to the uncoupled corrosion potential of the larger metal. For a welded stainless steel structure, the area of the weld metal is typically much less than the area of the substrate being welded, which means that the potential of the welded structure will be equal to the corrosion potential of the stainless steel in the particular environment. If the weld metal is less noble than the stainless steel, the galvanic coupling will result in an increase in the potential of the weld. This can result in aggressive attack of the weld if the stainless steel corrosion potential is above the breakdown potential of the weld, or if the less noble weld metal does not passivate and dissolves actively. However, if the weld metal is noble relative to the stainless steel, then the galvanic coupling will result in cathodic protection of the weld metal by the stainless steel. It is possible to use the fundamental principles outlined above to develop design criteria for a new weld metal for stainless steel:

1. The breakdown and repassivation potentials of the weld metal should be higher than the corrosion potential of the stainless steel base metal to prevent localized attack of the weld metal.
2. The corrosion potential of the weld metal should be slightly higher than that of the stainless steel base metal so that the weld metal is cathodically protected.

Guidance on galvanic interactions can be obtained by the galvanic series. The OCP of Monel K-400 is in the similar range as those of the austenitic stainless steels in seawater<sup>13</sup>, distilled water<sup>14</sup>, potable water<sup>14</sup>, HCl<sup>14</sup>, and H<sub>2</sub>SO<sub>4</sub><sup>14</sup>. Alloy 400, commonly known as Monel contains 31% Cu (typical value), and maximum concentrations of 2.5% Fe, 2% Mn, 0.5% Si, 0.3% C, and 0.024 % S<sup>15</sup>. Monel has good corrosion, erosion and cavitation resistance in seawater and is widely used in seawater under conditions of high flow velocity such as propellers, shafts, condenser tubes and heat exchangers<sup>16,17,18</sup>.

Also, Ni-Cu alloys do not generate deep pits during long-term exposure in chloride environments, but instead form shallow attack<sup>19,20,21,22</sup>. Therefore, Monel was chosen as the starting point for this study.

In this report, the behavior of stainless steel welded with Monel and the effect of Cu on the passivity of Ni-Cu alloys are presented. A subsequent paper will present work leading to an optimized consumable composition.

### **Experimental Procedure**

Welds were made using a 6.35 mm thick 304L (UNS S30403) base metal plate and 1.14 mm diameter commercial Monel (AWS ERCuNi) or standard 308L stainless steel (AWS ER308L) filler wire. The compositions of these materials are given in Table 1. Also shown in Table 1 are the calculated values of weld metal composition for 15 and 40% dilution for the case of 304L base metal and Monel filler metal. This represents a typical range for most arc welding processes. Note that dilution is defined as dilution of the filler metal by the base metal. Gas Tungsten Arc Welding (GTAW) was the welding process used in this study because it is easier to automate and control than SMAW, which is the most common process for manual welding of stainless steel. Details of the GTAW process are given in Table 2.

Corrosion testing was performed on welded samples and on buttons prepared by electric-arc melting of pure elemental mixtures. Five Ni-Cu alloys were manufactured, having Cu composition in the range of 25 - 45 wt.%. The buttons were then cold-rolled with a thickness reduction ratio of 75%. Finally, they were solutionized at 1100°C for 1 hour to result in homogenized microstructures.

The specimens for electrochemical testing were mounted in epoxy, polished to 600 grit paper, degreased in acetone, and then rinsed with distilled water. The edge between the specimen and epoxy mold was sealed with lacquer to reduce the likelihood of crevice corrosion.

For electrochemical tests, a computer-controlled potentiostat system was used with a Saturated Calomel Electrode (SCE) reference electrode and a carbon rod counter electrode. Air or Ar was bubbled through the solutions for aerated or deaerated conditions, respectively. Artificial seawater was produced according to ASTM D-1141-52. The pH was fixed at 8.3. For corrosion testing, samples were extracted from the welds so that the heat affected zone (HAZ), the weld interface, and base metal were exposed. Cyclic potentiodynamic polarization was performed at a scan rate of 10 mV/min in air-bubbled 0.1 M NaCl and artificial seawater at room temperature.

Long Time Exposure (LTE) testing was performed on the Ni-Cu alloys and welds in aerated artificial seawater and 0.1 M NaCl solution. The samples were polished to 600 grit paper and then spot-welded with Pt wires to allow them to be hung in the solutions and for making periodic electrochemical measurements. After degreasing in acetone, the bare Pt wire was coated with lacquer. For samples exposed in artificial seawater, the Pt/sample joint was not coated with lacquer to prevent any possibility of crevice

corrosion between the lacquer layer and specimen. However, for samples exposed in 0.1M NaCl solution, this joint was masked with black wax to prevent galvanic corrosion between the Pt wire and the sample. During the exposure, the corrosion potential and polarization resistance of each sample were periodically measured. After the exposure, the surfaces of the specimens were optically inspected and the corroded sites were analyzed with Scanning Electron Microscopy (SEM) and Energy Dispersive Spectroscopy (EDS). All tests were carried at room temperature.

The welds were analyzed by optical microscopy on polished sections that were electrolytically etched in 5 vol.% H<sub>2</sub>SO<sub>4</sub> and then in 50 vol.% HNO<sub>3</sub>. Weld ductility was tested by bending over a 3/4" mandrel, resulting in 15% tensile strain in the outer fibers. Vickers microhardness scans were performed across the welds.

## **Results and Discussion**

### **Weldability of Monel electrode**

Welds were made with 304L plate and Monel weld wire using a range of conditions. Solidification cracks were observed in high-dilution welds, but not if the weld dilution was kept below about 30%. The use of 100% Ar gas for shielding resulted in surface slagging and welds of unsatisfactory quality, Figure 1a. This slagging was worse at high heat inputs and seemed to be related to the presence of Ti in the Monel weld wire. The effect was eliminated by the use of Ar-5%H<sub>2</sub> shielding gas and control of weld heat input, Figure 1b. The weld metal was found to be fully austenitic with perhaps some second phase formation in the interdendritic regions<sup>23</sup>.

EDS line profiles from the base metal into the weld nugget of a particular Monel/304L weld indicated that there were about 10% Fe and a few percent of Cr in the weld nugget as a result of dilution, Figure 2. Also evident was a transition zone in which the composition gradually changed from the base metal to the weld metal.

A Monel/304L weld was tested by bending over at 1.9 cm mandrel. The sample passed this test with no evidence of cracking. Micro-hardness profiling was performed along the weld cross-section. The hardness of the Monel/304L weld metal was slightly below that of a weld made with 308L filler metal, Figure 3. Transverse tensile tests were performed on Monel/304L welds at nominally 25% dilution. All failures occurred in the weld metal. The average mechanical properties were as follows: 80 ksi tensile strength, 44 ksi yield strength, and 40% elongation. In summary, the Monel weld showed good ductility and strength as long as solidification cracking was by controlling the heat input.

Most of the welds exhibited three zones near the welding interface: partial liquation zone in the base metal, epitaxial growth zone in weld metal, and columnar structure in the weld metal, Figure 4. The grain boundaries in the epitaxial growth zone were well matched with those in base metal. The epitaxial growth zone was a little wider in high dilution samples than in low dilution samples. This might cause large micro-segregation in high dilution samples.

Around the welding interface, the range of compositional dilution is very wide as shown in Figure 2. Even for a low dilution weld, the interface is composed of the full range of dilution. To connect the composition measurements to the microstructure, EDS spot analysis was performed near the weld interface, Figure 5. The analysis at point A in the stainless steel base metal showed no change in composition. However, at point B in the heat affected zone (HAZ) near the weld, there was a slight increase in Cu and Ni and a slight decrease in Cr. It is not expected that the HAZ will have significant difference in corrosion resistance than the base metal. The epitaxial growth region, point C, was highly diluted zone with Fe and Cr. The initial columnar region, point D, showed a medium dilution level and the inner columnar region, point E, a low dilution level.

### **Long-time exposure tests**

LTE tests were carried out in artificial seawater for up to 50 days. The corrosion potentials were measured for 500 h. All samples exhibited ennoblement in corrosion potential with time, Figure 6. The five binary Ni-Cu alloys containing 25-45% Cu behaved similarly and exhibited corrosion potentials within about 0.05 V of each other. In the initial stage, the corrosion potential of Ni-45Cu was the highest of the five, but Ni-25Cu exhibited the highest potential in the later stages of exposure. The ennoblement of stainless steel 304L was the highest of all the specimens. A polished Monel/304L weld sample also exhibited ennoblement in the early stages of immersion but it became active after 2 days of immersion.

After immersion for 50 days, no corrosion was found on the binary Ni-Cu alloys samples containing 35% Cu or less, but pits were observed on the 40 and 45% Cu samples. Several pits were observed on the Monel sample, and they exhibited blue corrosion products that were likely Cu rich. However, since the Ni-30Cu binary alloy, which has the same Cu content as Monel, did not exhibit any corrosion, it is possible that the attack on Monel was caused by heterogeneities in the commercial rod product. Some contamination was generated on the surface of the stainless steel sample during LTE testing, but it was not corrosion product because it was easily removed by brushing. The polished weld also exhibited different forms of corrosion, Figure 7. Pits were found in the weld metal near the interface. Some of the pits were quite large, with diameters more than 100  $\mu\text{m}$ , but they were not deep. Intergranular corrosion (IGC) was found inside these pits, Figure 7e, and at some locations on the interface of the weld metal and base metal, Figure 7f. Some regions of heavy corrosion product were also found along the interface, Figure 7f.

In 0.1M NaCl solution, the corrosion potentials of the various samples were measured for 172 h. The corrosion potential of the Ni-25 Cu and Ni-30Cu binary alloys increased with time and reached a plateau of about 50 mV SCE, Figure 8a. The corrosion potentials for the other samples were lower, in the range of -50 to -100 mV SCE. After 172 h, the weld potential was the lowest. These results were similar to the data in artificial seawater except that the 304L sample did not exhibit the highest corrosion potential in 0.1 M NaCl as it did in seawater. For most of the exposure period, the corrosion potential of the polished-weld was between that of the Ni-30Cu alloy and stainless steel 304L. Polarization resistance ( $R_p$ ) measurements found that the  $R_p$  of the Ni-Cu alloys initially

increased with time and then decreased, Figure 8b. After 7 days, the  $R_p$  of stainless steel and pure Ni were the highest while that of Ni-45Cu alloy was the lowest. The  $R_p$  of the polished-weld was between those of stainless steel 304L and Ni-30Cu alloy.

After 14 days immersion in 0.1 M NaCl, potentiodynamic polarization tests were performed on three Ni-Cu alloys, pure Ni, stainless steel 304L, and a polished Monel/304L weld sample. As shown in Figure 9, all of the Ni-Cu alloys exhibited a higher OCP than stainless steel 304L. One of the important results is that weld still maintained a passive state after the 14-day LTE test. The OCP and breakdown potentials are summarized in Figure 10. For some of the Ni-Cu alloys, a sharp breakdown potential was not observed and the breakdown potential was taken to be the potential at the current density of  $100 \mu\text{A}/\text{cm}^2$ . For all samples, the OCP was lower than the breakdown potential, indicating the stability of passivity. Ni-30Cu had the widest gap and therefore the most stable passivity among the Ni-Cu alloys. The weld also exhibited a stable passivity range of 0.1V. The breakdown potential of the weld was almost the same as that of Ni-45Cu.

Attack in the form of localized breakdown was observed after polarization to high potentials (up to a current density of  $100 \mu\text{A}/\text{cm}^2$ ) above the breakdown potential. On these samples, most of the attack occurred in the weld metal, Figure 11. The attack was interdendritic in nature and looked similar to the columnar and dendrite microstructure found after etching the sample (Figure 4). The Ni-Cu binary system forms an ideal solid solution, and Cu has a higher melting point, so Cu is enriched interdendritically in the liquid phase during solidification and is then finally segregated along the columnar and dendrite boundaries<sup>24,25</sup>. Also, as heat input rate in welding process increases, the level of the segregation at the boundary will increase because of the slow cooling rate. Therefore, it is likely that the Cu-enrichment at the boundary will be higher for high dilution welds.

### **Effect of Cu**

The long-term exposure tests on the 304L/Monel welds indicated that they have good corrosion resistance to dilute chloride solutions open to air. No attack was observed after exposure to 0.1 M NaCl. However, purposeful attack of the weld by polarization in chloride solution to high potentials indicated that the most susceptible region of the weld is the Cu-rich interdendritic microstructure. Therefore, it is of interest to understand better the effects of Cu on the corrosion properties.

Potentiodynamic polarization measurements were made on polished samples in artificial seawater. The corrosion potential in aerated artificial seawater was found to increase with increasing Cu content of the binary alloys, Figure 12a. Monel 400 had a similar corrosion potential as Ni-30Cu. The corrosion potentials of the Monel/304L weld and 304L were slightly higher than the binary alloys in this solution. In deaerated artificial seawater, there was little effect of Cu on corrosion potential for the binary alloys. However, Monel and the weld exhibited much lower values.

The breakdown potentials measured in both aerated and deaerated artificial seawater decreased with increasing Cu content for the binary alloys, Figure 12b. Monel K400 exhibited lower breakdown potential than Ni-30Cu and the Monel/304L weld exhibited similar breakdown potentials as Ni-45Cu. The breakdown potential of stainless steel 304L was the highest.

The significant result from this analysis is that the corrosion potential of stainless steel 304L is lower than the breakdown potential of the weld in both 0.1 M NaCl and artificial seawater. From these data, it can be predicted that the weld will not corrode by the mechanism of galvanic corrosion. Furthermore, as the Cu concentration in Ni-Cu alloys with composition near Monel increases, the resistance to localized corrosion decreases. This finding is in line with the observation of the intergranular attack at the welds during long time exposure to artificial seawater since the interdendritic region is likely enriched in Cu.

To investigate the effect of the segregation on the corrosion properties in Ni-Cu alloys, two welds having different level of dilution were annealed at 1150°C for 1 h to homogenize the microstructure and then rapidly cooled. Both showed much higher breakdown potentials than as-welded samples with the same dilution, Figure 13. After annealing, the breakdown potentials of the two welds were increased by 50 - 80 mV. The fact that homogenization improved the breakdown behavior of the Monel/304L welds further supports the notion that micro-segregation of Cu dominates the corrosion resistance of Ni-Cu welds.

The corrosion potential of the Monel weld was lower than its breakdown potential in chloride solution even after long-term immersion. However, some ennoblement of the corrosion potential of this weld occurred and its breakdown potential was considerably lower than that of stainless steel. For applications involving long time exposure, this weld should have improved breakdown behavior. To develop optimized Cr-free consumables for welding of stainless steel, it is necessary to improve further the localized corrosion properties of the weld metal. The detrimental effects of Cu on the properties of the weld suggest that lower Cu contents would be beneficial. However, the Cu is beneficial for increasing the corrosion potential of the weld to minimize galvanic coupling with the stainless steel base metal. A subsequent report will show that 5-10% Cu is sufficient to ennoble the corrosion potential of Ni, and results in minimal degradation of the localized corrosion properties<sup>26</sup>. Noble element alloying is also beneficial<sup>26</sup>.

### **Conclusions**

- Good quality GTAW welds were achieved using Monel (ERNiCu-7) filler metal and Type 304L base metal by controlling shielding gas and weld heat input.
- The strength and ductility of Monel/304L GTA welds were comparable to those of 308L/304L welds. Weld solidification cracking was observed at high heat inputs and dilution levels, but could be eliminated by restricting dilution below about 30%.

- Corrosion potentials generally increased during immersion in aerated chloride solutions. Polished welds exhibited this ennoblement in the early stage of immersion, but then the corrosion potential decreased, indicating some activation.
- No corrosion was observed on the weld sample or any of the alloys tested after long term exposure to 0.1 M NaCl. However, some localized corrosion of the weld was observed after long term exposure to artificial seawater.
- Sharp line attack was observed at the base-metal/weld-metal interface as a result of compositional dilution and accompanied microstructural heterogeneities. Large and shallow pits were found in the weld metal.
- At the columnar structures in the weld metal, micro-segregation of Cu occurred. Interdendritic regions are attacked during potentiodynamic polarization to high potentials, indicating an increased susceptibility associated with high Cu content.
- As the Cu content in Ni-Cu alloys increases, the corrosion potential increases but the breakdown potential decreases. The corrosion potential of weld is lower than breakdown potential.
- Ni-Cu alloys are possible candidates for Cr-free consumables for welding 304L stainless steel.

#### **Acknowledgements**

This work was supported by SERDP (Strategic Environmental Research and Development Program) through project PP-1346 and under the direction of C. Pellerin.

#### **References**

1. Mortazavi, Seyed B., *Welding in the World* 39, 6 (1998): p. 297.
2. Gray, C. N.; Hewitt, P. J.; and Dare, P. R. M., *Welding & Metal Fabrication* 50, 8 (1982): p.393.
3. Gray, C. N.; Hewitt, P. J.; and Dare, P. R. M., *Welding & Metal Fabrication* 51, 1 (1983): p. 52.
4. Pierre-Jean Cunat, *Materiaux & Techniques* 90, 1-2 (2002): p.19.
5. "Welding Fumes and Gases" National Occupational Health and Safety Commission, Australian Government Publishing Service, Canberra 1990.
6. E. Zumelzu and C. Cabezas, *J. Mat. Proc. Tech.* 57 (1996): p. 249.
7. S. A. Campbell, G. J. W. Radford, C. D. S. Tuck, and B. D. Barker, *Corrosion* 58, 1 (2002): p. 57.
8. J. R. Scully and H. P. Hack, in *Galvanic Corrosion*, ASTM STP 978, edited by H. P. Hack (ASTM, Philadelphia, 1988): p. 136.
9. J. A. Ellor and J. G. A. Gehring, *MP* 27, 5 (1988): p. 45.
10. U. Xue, N. Xu, and C. Zhang, *Advances in Contraception* 14, 2 (1998): p. 153.
11. H. I. A. Hossani, T. M. H. Saber, R. A. Mohammed, and A. M. S. E. Din, *Desalination* 109, 1 (1997): p. 25.

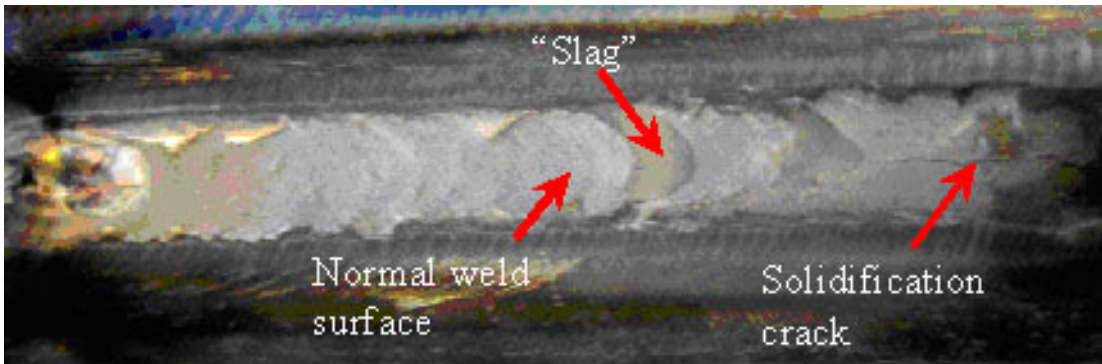
12. B. Wallen and T. Andersson, in Galvanic corrosion of copper alloys in contact with a highly alloyed stainless steel in seawater, held June 2-4, 1986 (Stockholm, Sweden, Swedish Corrosion Institute), p. 149.
13. ASM Hand book, Vol.13: Corrosion, 9th ed. (Materials Park, OH: ASM International, 1987), p. 234.
14. J. R. Crum and R. C. Scarberry, in Development of galvanic series in various acid and water environment, Corrosion of Ni-base alloys, held Oct. 23-25, 1984 (Cincinnati, OH, ASM), p. 53.
15. C. R. Southwell and A. L. Alexander, MP 8,3 (1969): p. 39.
16. H. H. Uhlig and R. W. Revie, Corrosion and Corrosion Control, 3rd ed. (John Wiley & Sons, New York, 1985).
17. J. A. Carew and M. Islam, MP 34, 4 (1995): p. 54.
18. R. W. Revie, Uhlig's Corrosion Handbook (John Wiley & Sons, Inc., Pennington, 2000).
19. E. A. Baker, in Degradation of Metals, ASTM STP 965, edited by S. W. Dean and T. S. Lee, (ASTM, Philadelphia, 1988): p. 125.
20. B. S. Phull and R. M. Kain, in Corrosion resistance of nickel-containing engineering materials in marine environments, Nickel-Cobalt 97 International Symposium, held Aug. 17-20, 1997 (Sudbury, Ontario, Canadian Institute of Mining, Metallurgy, and Petroleum), p. 141.
21. V. B. Singh and A. Gupta, J. Mat. Sci. 36, 6 (2001) p. 1433
22. J. L. Luo and M. B. Ives, J. Electrochem. Soc. 144, 11(1997): p. 3907
23. J.C. Lippold, G. Guaytima, G.S. Frankel, and Y.H. Kim, "Development of Ni-Cu Filler Metals for Joining Austenitic Stainless Steels," Stainless Steel World 2004, KCI Publishing BV, Zutphen, The Netherlands, pp. 140-148.
24. M. Hasebe and T. Nishizawa, in Application of Phase Diagrams in Metallurgy and Ceramics, Vol. SP-496, held Jan. 10-12, 1977 (Gaithersburg, MD, National Bureau of Standards), p. 911.
25. B. Prakash, J. Electrochem. Soc. India 27, 2 (1978): p. 101.
26. Y.H. Kim, G. S. Frankel, J.C. Lippold, and G. Guaytima, to be submitted to Corrosion.

Table 1. Composition of Monel filler metal and 304L base metal composition range for 308L SS filler metal. Calculated weld metal composition for 304L/Monel welds at 2 different dilutions are also given and threshold composition values for weldability.

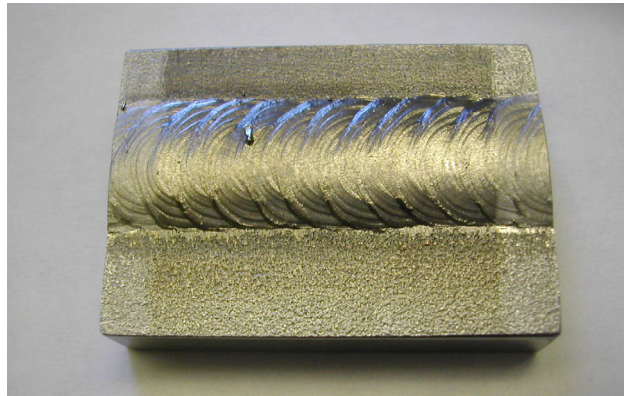
Element (wt%)	Monel Wire	304L SS	308L SS	15% Dilution calculated	40% Dilution calculated
Ni	63.99	8.08	9-11	55.60	41.63
Cu	28.81	-	0.75 max	24.49	17.29
Fe	0.76	72.10	65	11.46	29.30
Cr	-	18.09	19.5-22.0	2.71	7.24
Mn	3.49	1.24	1.0-2.5	3.15	2.59
Ti	1.99	-		1.69	1.19
Si	0.90	0.37	0.3-0.65	0.82	0.69
N	-	0.06		0.01	0.02
C	0.05	0.03	.08 max	0.05	0.04
Others	0.01	0.03		0.01	0.02

Table 2. Details of GTAW procedure

Current	150 Amp
Voltage	12 V
Travel speed	5 in/min
Heat input	21.6 kJ/in (0.85 kJ/mm)
Wire feed speed	45 in/min
Shielding gas	Argon + 5% H <sub>2</sub>
Shielding gas flow rate	30 ft <sup>3</sup> /min
Joint design	V- groove 90°, gap: 0.118 in



a)



b.

Figure 1. Monel/304L welds made using GTAW. a) Surface slagging and solidification cracking exhibited by high heat input welds with Ar shielding gas exhibited b) Good quality welds produced with 95Ar-5% $H_2$  shielding gas.

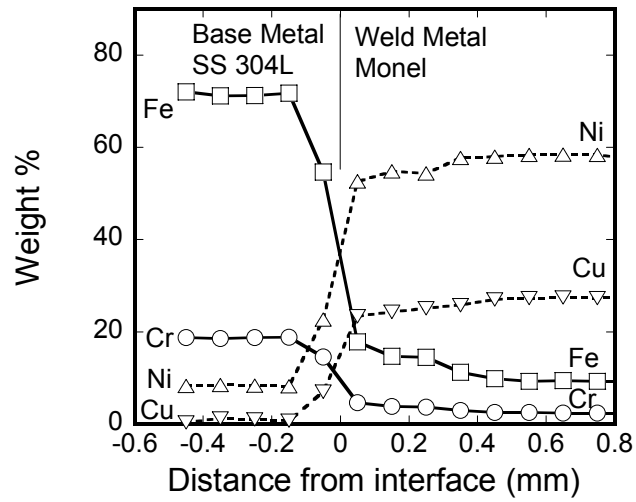


Figure 2. Compositional profile at the weld interface determined by EDS profiling.

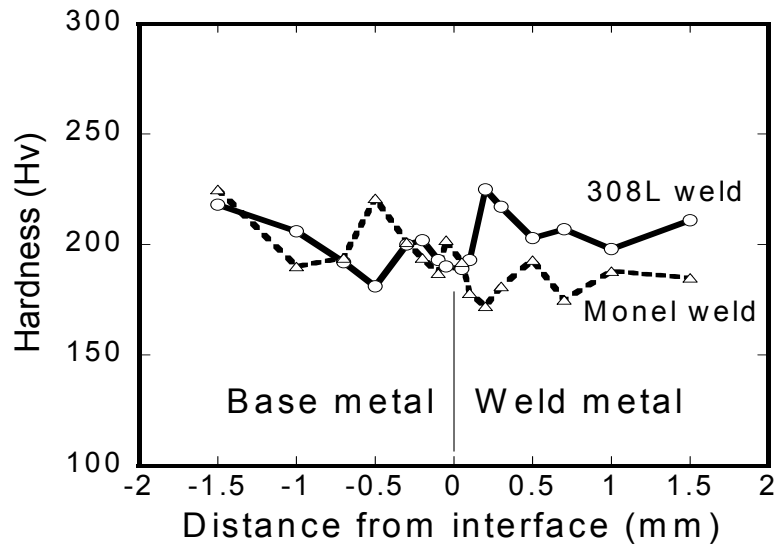


Figure 3. Microhardness traverses from the base metal (left) into the weld metal for Monel/304L and 308L/304L GTA welds.

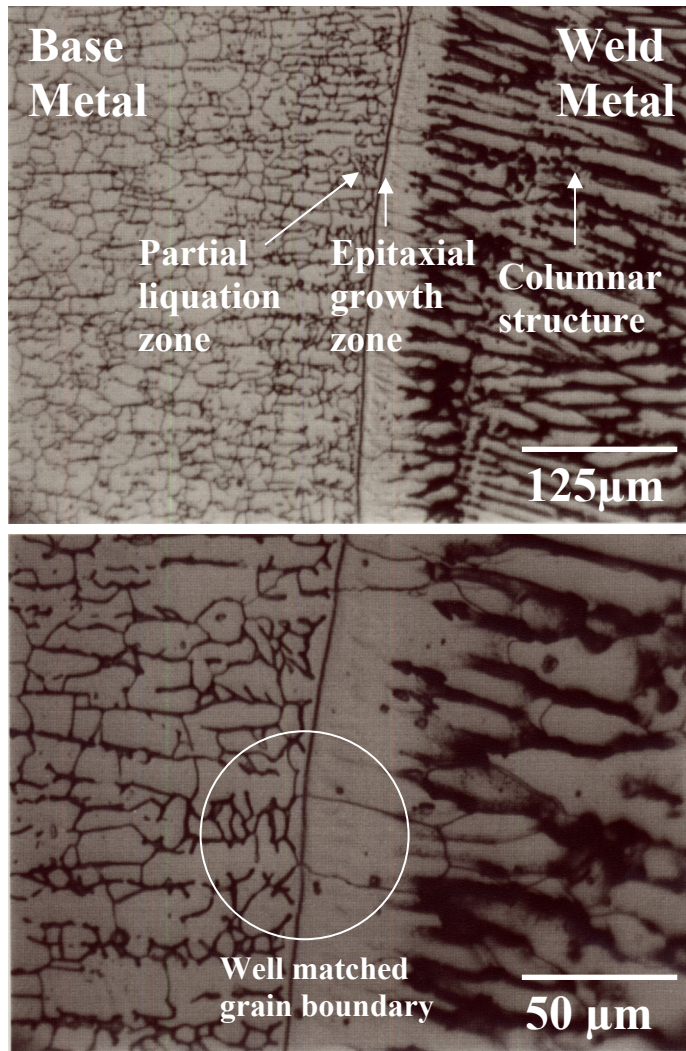
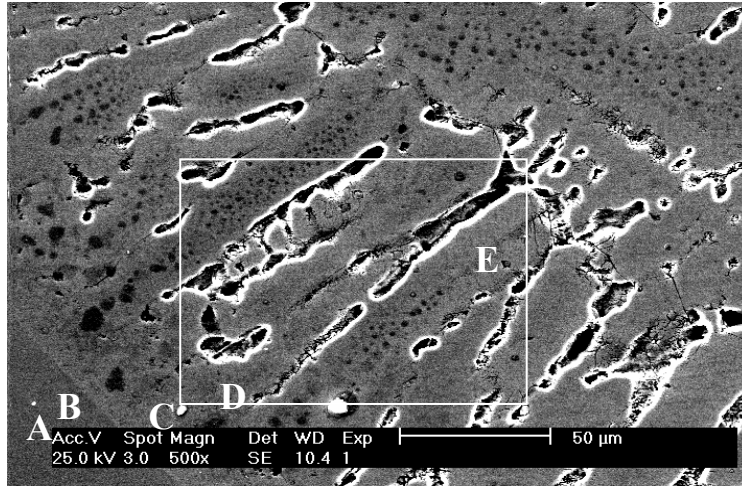


Figure 4 Optical micrographs of Monel/304L weld at two magnifications. Heat input 42KJ/in, dilution 53%.



Wt.%	Ni	Cu	Fe	Cr	Mn	Si	Ti
A	7.8	0.1	71.4	18.5	1.5	0.7	-
B	9.6	0.5	68.9	17.5	1.5	0.8	-
C	55.0	17.9	18.2	4.7	2.1	0.9	1.2
D	57.9	19.4	13.9	3.6	2.8	0.9	1.5
E	55.1	23.0	11.1	3.1	3.8	1.4	2.0

Figure 5 SEM-EDS spot analyses across the Monel/304L weld interface including spots in the base metal (A, B) and weld metal (C, D, E)

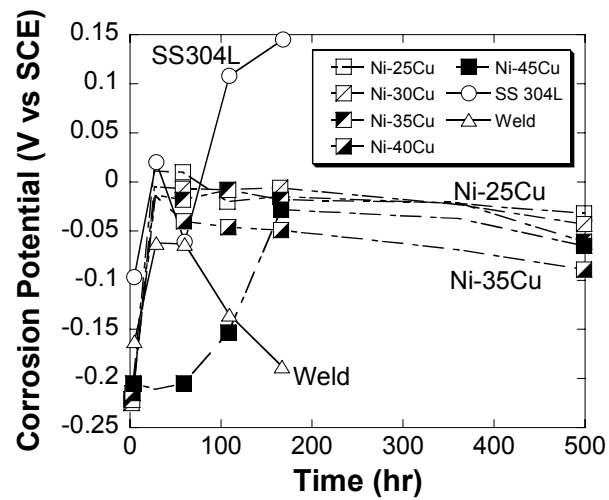
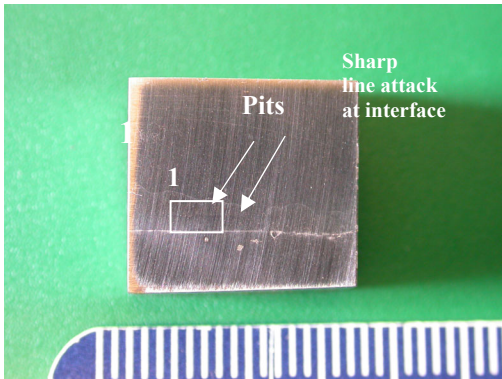
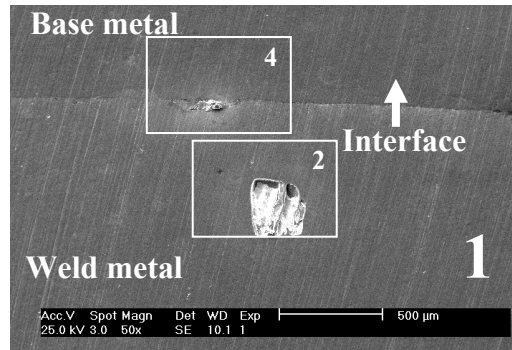


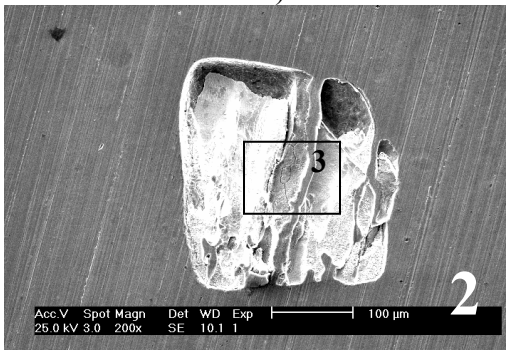
Figure 6. The corrosion potentials of the binary Ni-Cu alloys, 304L stainless steel, and a Monel/304L weld during immersion in aerated seawater.



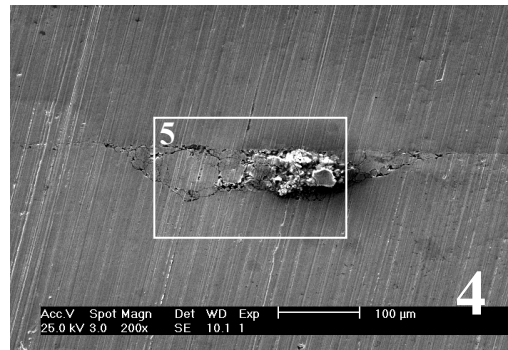
a)



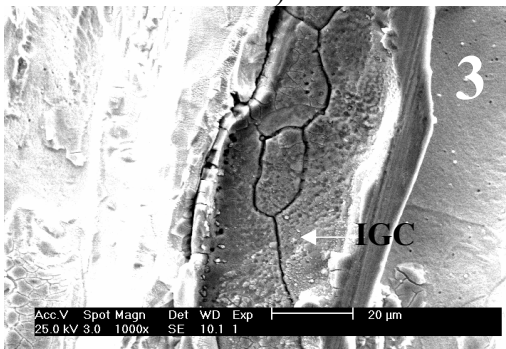
b)



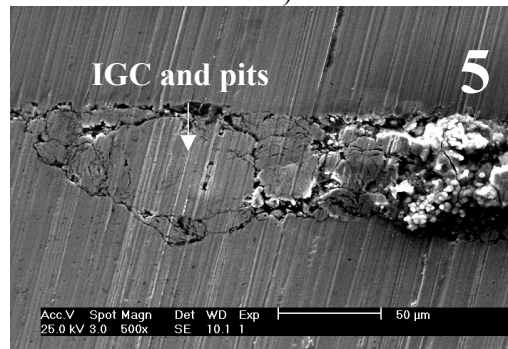
c)



d)

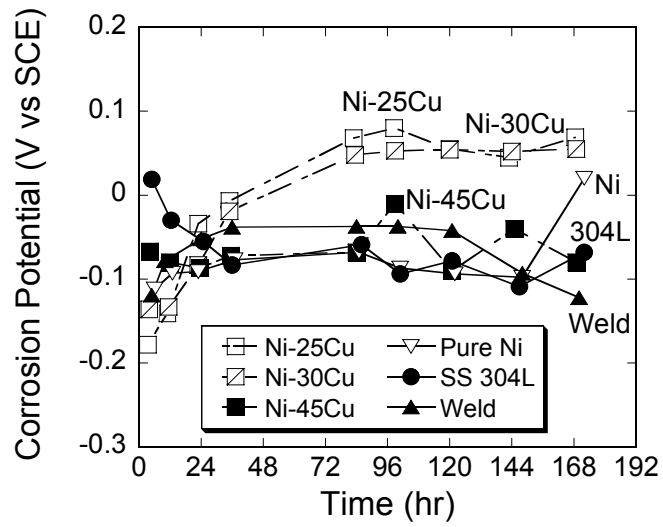


e)

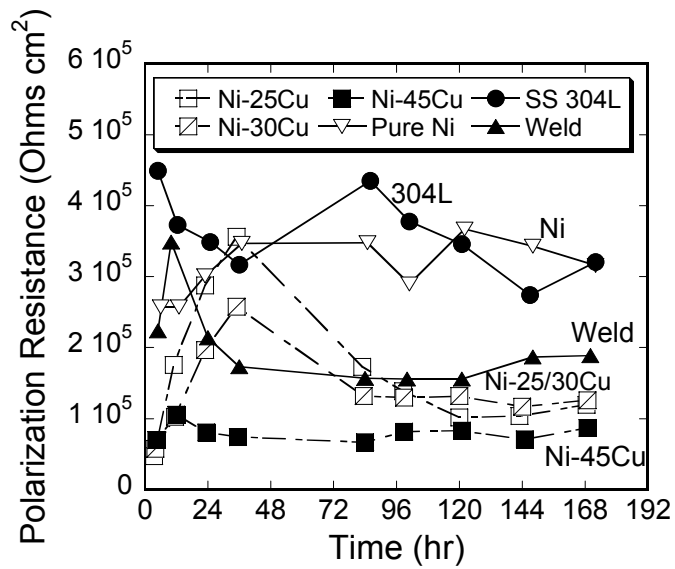


f)

Figure 7. Images of the Monel/304L weld following 50 days in artificial seawater. a) low magnification optical image (each division in scale is 1 mm) b) SEM image of the box marked 1 in a. Note the large shallow pit in the weld metal (box 2) and the heavy corrosion product at the interface (box 4) c) SEM image of the box marked 2 in b. d) SEM image of the box marked 4 in b. e) SEM image of the box marked 3 in c. Note the intergranular corrosion in a region of the pit. f) SEM image of the box marked 5 in d. Note the intergranular corrosion and the heavy corrosion product.



a)



b)

Figure 8. Exposure of the binary alloys, 304L, pure Ni, and Monel/304L weld in 0.1M NaCl for 172 h. a) corrosion potentials b) polarization resistance

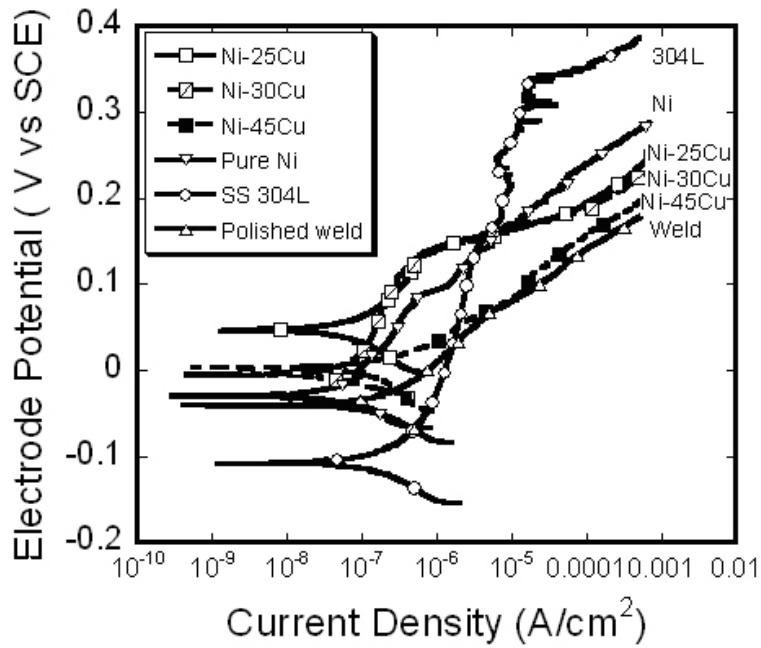


Figure 9. The polarization behavior of resistance of the Ni-Cu alloys, stainless steel steels, pure Ni, and the polished-weld in 0.1M NaCl after 14 days LTE test

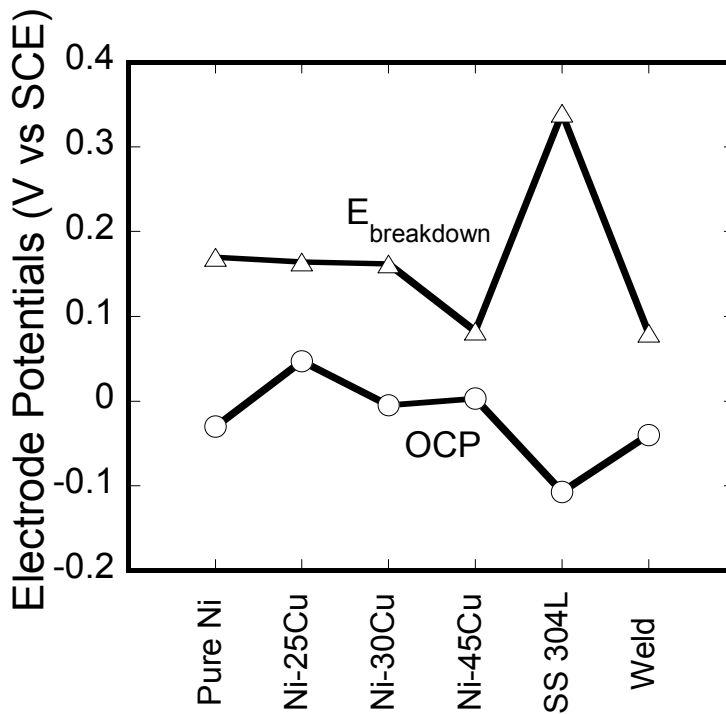


Figure 10. The open circuit potential and breakdown potentials of several alloys after LTE test.

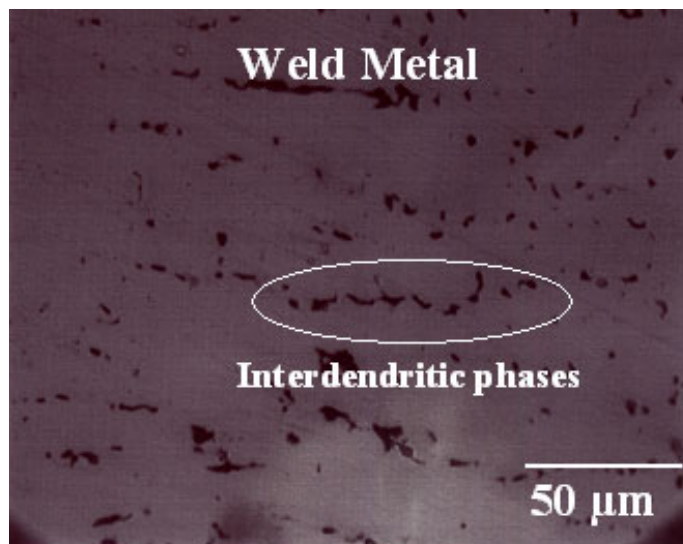
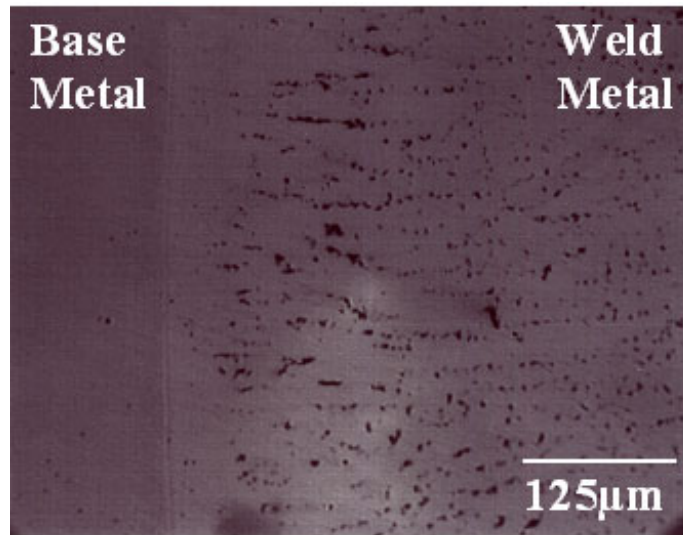
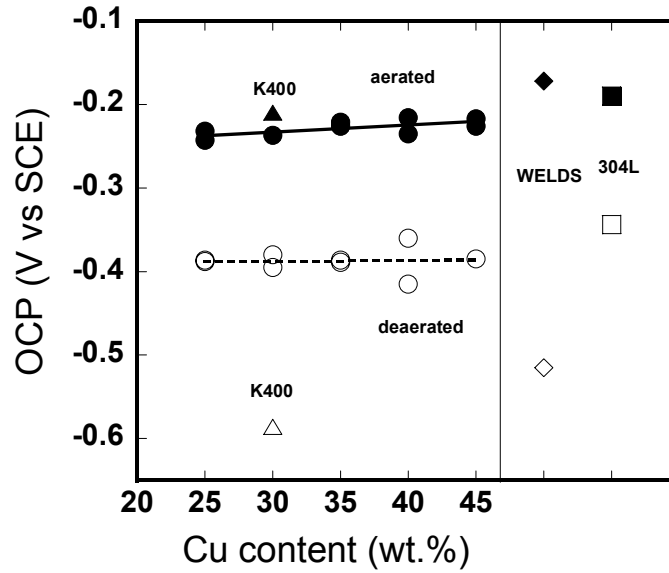
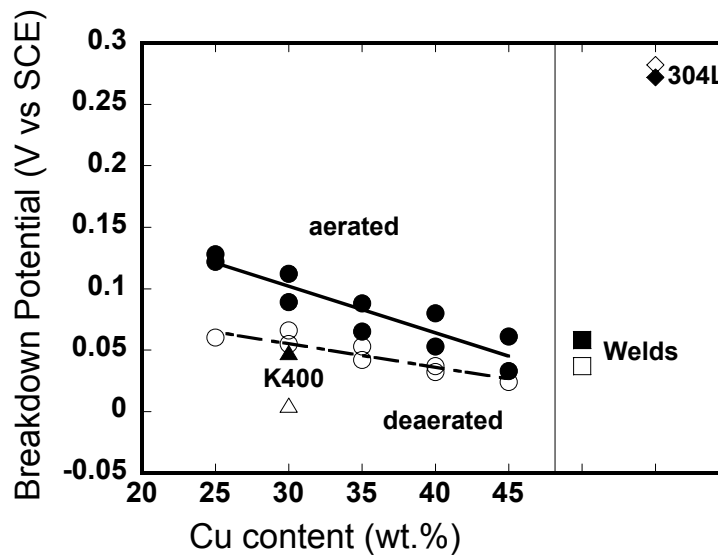


Figure 11. Optical micrographs of weld metal in Monel/304L after potentiodynamic polarization to  $100\mu\text{A}/\text{cm}^2$  in 0.1M NaCl solution. Heat input 36KJ/in, Dilution 43%.

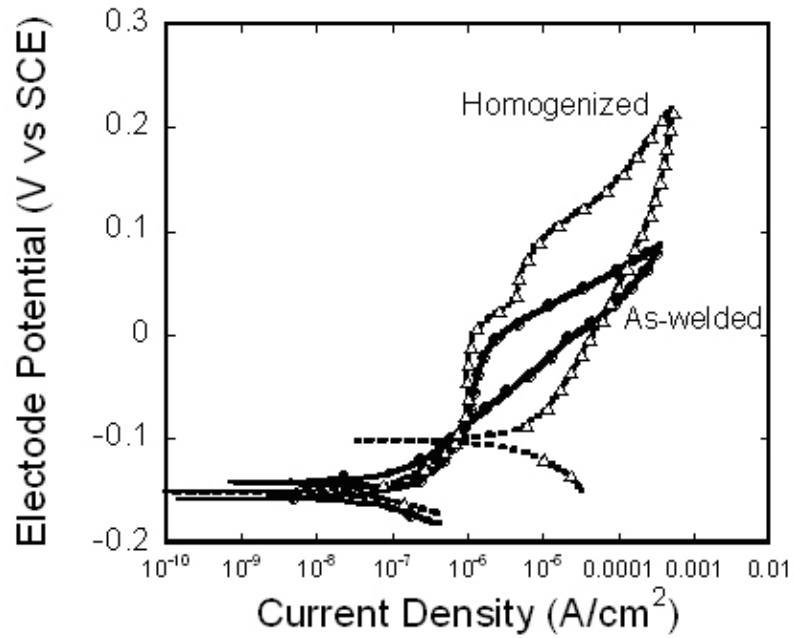


a)

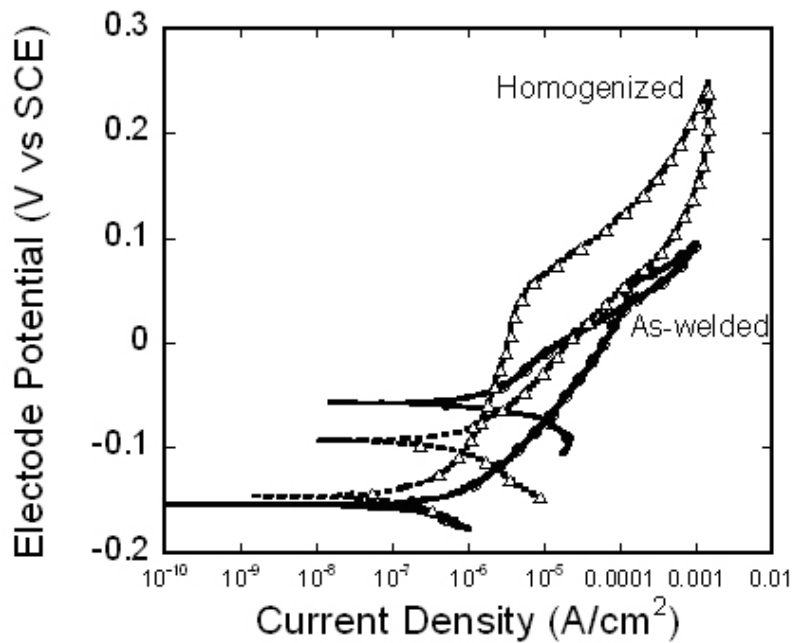


b)

Figure 12. Effect of Cu content on results from potentiodynamic polarization curves for Ni-Cu alloys and weld in artificial seawater. open symbols – deaerated, closed symbols – aerated. a) open circuit corrosion potential b) breakdown potential



a)



b)

Figure 13. Effect of the homogenization treatment on the breakdown behavior of welds with different amounts of dilution. a) 12% dilution, b) 24% dilution

## Cr-free Consumables for Welding Stainless Steel. Part 2: Optimization of Alloy Composition Based on Corrosion Behavior

Yeong Ho Kim\*, G. S. Frankel\*, and J. C. Lippold\*\*

\*Fontana Corrosion Center, Dept. of Materials Science and Engineering

\*\*Dept. of Industrial, Welding, and Systems Engineering

The Ohio State University

Columbus, OH 43210

### Abstract

The effects of alloying elements on the corrosion properties of Ni-Cu alloy were investigated to optimize the composition of a Cr-free consumable for welding of stainless steels. Cyclic polarization experiments were performed in 0.1 M NaCl on Ni-base alloys containing different amounts of Cu, Pd, Mo, Fe, and Cr. The localized corrosion behavior, as exhibited by the breakdown and repassivation potentials, improved as the Cu content decreased from 30 to 5 wt% for both of as-cast and homogenized Ni-Cu alloys. The addition of Mo up to 10 wt% resulted in a detrimental influence on the localized corrosion with a decrease of the breakdown potential. Additions of Fe and Cr were studied to examine the effects of weld metal dilution by the stainless steel base metal. These elements slightly increased the breakdown potential, but decreased the repassivation potential. The micro-enrichment of Cu at the columnar boundary and intermetallic compounds in the weld degraded the behavior of localized corrosion for as-cast Ni-Cu alloys and for welds based on Ni-Cu alloys. The addition of 1 wt% Pd ennobled the alloy and greatly improved the localized corrosion properties. The optimized composition for a new welding consumable is a Ni-based alloy containing 5-10 wt% Cu and 1 wt% Pd. This alloy exhibited slightly higher corrosion potential, slightly lower breakdown potential, and much higher repassivation potential compared to type 304L stainless steel.

Keywords: Welding, Corrosion, Stainless steel, Nickel, Copper, Palladium, Molybdenum, Dilution, Segregation, Breakdown, Repassivation

Contact info: GS Frankel, 477 Watts Hall, 2041 College Rd. Columbus, OH 43210 tel: 614-688-4128, fax 614-292-9857, frankel.10@osu.edu (until June: Max Planck Institute fur Eisenforschung, Max-Planck-Str. 1, D-40237, Duesseldorf, Germany)

### Introduction

In a previous study<sup>1</sup>, the rationale for finding Cr-free consumables for welding stainless steel was presented. Based on the consideration that the corrosion of a welded structure containing a dissimilar weld material will be governed by galvanic corrosion, the following design criteria were presented: 1) The breakdown ( $E_B$ ) and repassivation ( $E_R$ ) potentials of the weld metal should be higher than the corrosion potential ( $E_{CORR}$ ) of the stainless steel base metal to prevent localized attack of the weld metal. 2)  $E_{CORR}$  of the weld metal should be slightly higher than that of the stainless steel base metal so that the weld metal is cathodically protected. It was shown that Monel (Ni-30Cu) exhibited an  $E_B$  in dilute chloride environments that was higher than the  $E_{CORR}$  of type 304L stainless

steel and that 304L/Monel welds survived long time exposure to aerated dilute chloride solutions. However, the localized corrosion behavior of the Monel weld was considerably worse than that of stainless steel because of its relatively low  $E_B$ <sup>1</sup>. Furthermore, the Cu-rich regions in the weld were susceptible sites for localized corrosion. Therefore, there is a need to find an optimized consumable composition with improved resistance to localized corrosion.

There have been many studies investigating the role of alloying elements on the corrosion resistance of Ni-Cu alloys. Regarding the effect of Cu, it was found that the corrosion resistance of Ni-Cu alloy was superior to pure Ni only in the active region<sup>2</sup>. The behavior of Ni-Cu alloys containing 0-100 wt% Cu were studied in 10% HCl, 3% NaCl, and 10% HNO<sub>3</sub> and the alloy with about 30 wt% Cu was found to exhibit the lowest corrosion rate<sup>3</sup>. However, alloys with Cu content between 0 and 20 wt% were not studied. The passive region in experimentally-determined Pourbaix diagrams for Cu-(0-75%)Ni alloys in Cl<sup>-</sup>-containing solutions was enlarged in the acidic region as the Cu content decreased<sup>4</sup>. For Ni-(10-90 wt%)Cu alloys, the critical content of Ni, above which passivation was easily achieved, was found to be about 40 wt%<sup>5</sup>. Cu was found to selectively dissolve from Ni-Cu alloys with 30-50 wt% Cu in natural seawater<sup>6</sup>. Ni improved the passivity of the Ni-Cu alloys in NaOH solutions and inhibited the dissolution of Cu<sup>2+</sup> ions<sup>7</sup>. The weight loss in quiescent seawater over 2 years was found to increase as the Cu content in Ni-Cu alloys increased<sup>8</sup>. The increase of Cu content from 30 to 53 wt% increased the weight loss but decreased the pitting depth of Ni-Cu alloys in the same environment<sup>9</sup>. A low Cu content in Ni-Cu alloys promoted the formation of a protective Ni(OH)<sub>2</sub> film, and the dissolution of Cu was inhibited in alkaline solution<sup>10</sup>. In summary, many studies have shown that Cu exerts harmful effects on the passivity of the Ni-Cu alloys in neutral and alkaline solutions but could reduce active dissolution in acidic environments. This suggests that there might be optimum range of Cu content in Ni-Cu alloy having the best resistance to passivity breakdown.

Other alloying elements are also of interest. Like Ni and Cu, Pd has a face centered cubic (FCC) crystallographic structure and is known as one of the less expensive Platinum Group Metals (PGMs). Pd is inert in many environments, and is very effective as a hydrogenation catalyst.<sup>11</sup> Tomashov and Chernova summarized the effect of noble metals on the passivity of cathodically modified alloys<sup>12</sup>. Pd as a noble metal was found to enhance the cathodic reaction so that Pd additions to Ti-, Cr-, Zr-based alloys, and stainless steels resulted in higher corrosion potential and lower weight loss in different acidic environments<sup>12,13</sup>. The reduced corrosion rate is essentially a result of anodic protection, or polarization of the metal to higher potentials in the passive region. Andresen et al. studied the effect of Pd on the growth of the oxide on Ni-base alloys<sup>14-16</sup>. Doping of the noble Pd in the oxide film improved the life of the oxide in a deaerated aqueous environment at 288°C. It was also found that Pd incorporation into the growing oxide on the surface of austenitic stainless steel improved the resistance to SCC.<sup>17</sup> Potgieter studied the cathodic modification of alloys with noble metals<sup>18</sup>. The noble metals provided a high exchange current density for the reduction reaction, which shifted the open circuit potential (OCP) to the passive range resulting in easy passivation. The effectiveness of this modification was best for PGMs and was ordered in terms of high

effectiveness from Pt to Pd, Ir, Ru, and Os. He found that the noble metal was enriched on the surface after active dissolution and that Mo had a synergetic effect with PGMs. The addition of 0.1% Pd to pure Cr lowered the corrosion rate by a factor of  $10^5$ , by enriching at active sites such as kinks where the active dissolution of Cr preferentially occurred. The addition of Au, Pt, or Pd ennobled the OCP of type 316 stainless steel in 1N  $H_2SO_4$  solution for 150 hours, and enrichment of these noble metals was detected on the surface<sup>19</sup>. Ennoblement of the OCP and low passive/active current densities were also reported for Fe-25Cr and Fe-18Cr-10Ni with the enrichment of Pd on the surface by electrolytic deposition<sup>20</sup>. Therefore, the literature suggests that the addition of Pd into Ni-Cu alloys could enoble the OCP and improve the breakdown behavior.

Mo is known as a corrosion-resistant element in reducing environments<sup>21, 22</sup>. However, Mo-containing Ni-Cu alloys exhibited somewhat nobler OCPs and much lower charge transfer resistance ( $R_{ct}$ ) compared to those typical of Monel-400<sup>23</sup>. In a study on the effects of Mo in pure Ni and pure Fe in 1N  $H_2SO_4$  at 50°C, the primary passive potential and the passive current increased with increasing the content of Mo from 0 through 10 wt%<sup>24</sup>. Mitrovic-Scepanovic and Ives studied the passive behavior of Ni-(0-22)Mo alloys in 0.15 N  $Na_2SO_4$  at pH 2.8<sup>25, 26</sup>. With the addition of less than 5 wt% Mo into Ni alloys, the passive film became unstable as a result of the creation of many Ni-site vacancies by the doping effect of Mo in the NiO film, and the passive current increased. It was reported that the Mo enriched at the surface of Ni-(0.1~8 wt%)Mo alloys<sup>27</sup>, and that addition of Cu and Mo into Ni alloys improved the corrosion resistance in the  $H_2SO_4$  solution<sup>28</sup>. Moriya and Ives reported that Mo was segregated at the surface during pitting of the Ni-13Mo alloy<sup>29</sup>. They detected a higher content of Mo inside pits than on the unpitted surface, which suggested that Mo inhibited localized corrosion. Cortes et al. found that the density of the passive NiO layer on Ni-(10 at%)Mo alloy after passivation in 1 M  $H_2SO_4$  solution was lower than that of the bulk oxide, and a high content of Mo was detected at the metal/oxide interface<sup>30</sup>. They proposed that Mo enhanced the disorder in the passive film of Ni-Mo alloys. The passive films on pure Ni and Ni-10Mo alloy in 1 M  $H_2SO_4$  were found to be composed of ordered NiO with the enrichment of Mo on the surface<sup>31</sup>. Kozlova et al. studied the phase diagrams of the Ni-Cu-Mo systems and found the solubility of Mo in Ni-30Cu alloy to be about 10-15 wt% at 900°C<sup>32, 33</sup>. The solubility of Mo in the Ni-Cu system increased with increasing Ni content at 1200°C<sup>34</sup>. Gupta found that Ni-Mo alloys were solid solutions without the formation of secondary phases with up to 15 at% Mo at 800°C<sup>35, 36</sup>. In summary, previous studies have found that Mo could have harmful or beneficial effects on the passivity of Ni alloys.

During the welding of stainless steel with a dissimilar weld metal, a considerable level of dilution of the weld metal by the stainless steel base metal is possible, especially at the welding interface where there are steep gradients between the two compositions<sup>1</sup>. The incorporation of the elements from the stainless steel into the Ni-Cu alloy weld metal can cause the formation of intermetallic compounds that can also change the corrosion properties. From the calculation of the impurity-impurity interaction energies, the Ni-Cu and Ni-Cr systems were solid solutions, but the Ni-Fe system formed intermetallic compounds<sup>37-39</sup>. The Cu-Cr and Cu-Fe systems were also predicted to form a segregated phases. Lopez-Hirata et al. observed spinodal decomposition of Cu-45Ni-10Cr into a Cu-

rich phase (69Cu-29Cr-2Ni) and a Ni-Cr rich phase (20Cu-60Ni-20Cr) during aging at 600-800°C<sup>40</sup>. The maximum solubility of Cr in Ni-30Cu was predicted to be about 10 wt% or less. Gupta et al. experimentally established the ternary phase diagrams of Ni-Cu-Cr systems, where the solubility of Cr in the Ni-30Cu system was less than 0.2 wt% at 400°C<sup>41</sup>. They found formation of the secondary phase  $\gamma_1$  in Ni-Cu-Cr systems, which was Cr-rich and had the same FCC crystallographic structure as the Ni-rich phase  $\gamma_2$ . Therefore, the dilution of Cr in the Ni-Cu weld metal could cause the formation of the Cr-rich secondary phase, which could affect the corrosion properties.

Lopez-Hirata et al.<sup>42</sup> observed spinodal decomposition of the Cu-Ni-Fe alloys into Cu-rich and Ni-rich phases. In the ternary phase diagrams of the Fe-Cu-Ni system at 400-1050°C, the solubility of Fe in the Ni-30Cu system was about 20 at% at 800°C and 2 at% at 400°C, and spinodal decomposition of  $\gamma_1$  and  $\gamma_2$  was predicted<sup>43,44</sup>. It was also reported that the solubility of Fe in the Ni-30Cu was about 20 at% or less at 850°C<sup>45</sup>. Therefore, dilution of Fe from the base metal into the weld metal might result in the formation of Fe-rich secondary phases.

In summary, Fe and Cr enhanced the formation of secondary phases during solidification when added over their solubility limits<sup>40-42, 44-47</sup>. The cooling rate during weld solidification can affect the distribution and composition of secondary phases, but it seems possible that secondary phases such as Fe-rich, and Cr-rich intermetallic compounds can be formed by dilution during the welding of stainless steel with Ni-Cu consumables.

To summarize the various effects of alloying on Ni-Cu alloys, increasing the Cu content can degrade passivity and its breakdown. Pd can ennoble the OCP of Ni-Cu alloys and enhance passivity. Pd is completely soluble in the Ni-Cu system without the formation of secondary phases. The role of Mo in the passivity of Ni-Cu alloys is ambiguous as Mo additions might improve or degrade the passivity of Ni-Cu alloys. The solubility of Mo in the Ni-Cu system is large enough to add up to 10 wt% in Ni-30Cu. The effects of Fe and Cr on the formation of secondary phases and on the corrosion resistance of the Ni-Cu alloys are still unclear. Fe and Cr can change the corrosion resistance of the Ni-Cu alloys by themselves and also by the formation of secondary phases during solidification.

In this report, the effects of Cu, Pd, Mo, Fe, and Cr content on the localized corrosion behavior of Ni-Cu alloys are presented. An optimum composition for Cr-free welding consumables is proposed based on corrosion considerations. A subsequent paper will present the results of simulated and real welds made in type 304L stainless steel with this newly developed alloy.

### **Experimental Procedures**

Welds were made using a 6.35 mm thick 304L (UNS S30403) base metal plate and 1.14 mm diameter commercial Monel (AWS ERCuNi) or standard 308L stainless steel (AWS ER308L) filler wire. Different levels of dilution were created by changing the weld heat input rate from 20 to 42 KJ/in, resulting in dilution from 12 - 60 %, Table 1. Solidification cracks were observed for the welds with high heat inputs of 43 and 60

KJ/in, which was dependent on the level of dilution<sup>1</sup>. Details of the welding process were given in the previous paper<sup>1</sup>. Pieces with equal areas of weld metal and base metal were machined from the welded plates for electrochemical testing. These samples were mounted in epoxy and polished with abrasive paper to 600 grit.

Buttons were prepared by electric-arc melting of pure elemental mixtures to result in a sample weighing about 10 g. Table 2 shows the composition of 24 homogenized alloys prepared with a Ni:Cu ratio of 7:3 and different compositions of Pd, Mo, Fe, and Cr. This part of the study focused on compositions similar to Monel (UNS MO400), which was the starting point of the previous study<sup>1</sup>, and has Ni and Cu in this ratio. In the previous study, the effects of Cu content from 25 to 45 wt% were presented<sup>1</sup>. To complement that work, a Ni-20 wt% Cu sample was prepared. Pd was added up to 2 wt%, and the highest amount of addition of Mo was 10 wt%, which should be close to the solubility limit<sup>34-36</sup>. To investigate the synergetic effects of Mo and Pd, samples with different ratios of Pd and Mo were also prepared. The effects of dilution were studied in these samples by adding Fe and Cr, both separately and together. These samples were homogenized to study only the effect of the alloying elements and eliminate other metallurgical influences such as segregation and microstructural heterogeneities. After solidification, the buttons were cold-rolled with a thickness reduction ratio of 75% and then solutionized in a vacuum at 1100°C for 1 h. One batch of these samples was water-quenched after solutionizing to quench in the homogenized structure and another batch with identical composition was furnace-cooled to study the effect of any intermetallic compounds that might form during the slow cooling.

Table 3 shows the composition of another batch of samples that were tested in the as-cast condition, which simulates the microstructure of real welds. The button-melter can produce almost the same microstructure as found in real welds because the cooling rate of the button is similar to the weld metal during welding. After solidification in the arc-melter, about 0.5 mm was ground off the bottom of each button prior to corrosion tests. In this group, the range of Cu content extended from 30 wt% down to 0 wt%, i.e. pure Ni, to investigate the effect of the small amounts of Cu. Based on the behavior of this set of binary alloy samples (see below), the Ni-5Cu and Ni-10Cu alloys were chosen, and samples were fabricated with 5 or 10 wt% Cu and the addition of 3 wt% Mo, 1 wt% Pd, and combinations of Mo and Pd. Finally, Ni-5Cu-1Pd and Ni-10Cu-1Pd were selected, and buttons of each were fabricated with 25 % or 50% dilution by stainless steel (using small chips of 304L SS added to the mixture of elements). All of the buttons in Table 3 were tested in the as-cast condition.

The samples for electrochemical testing were prepared using the same method in the previous study<sup>1</sup>. Cyclic potentiodynamic polarization was performed at a scan rate of 10 mV/min in air-bubbled 0.1 M NaCl at room temperature. The breakdown potential was considered to be the potential when the current density reached at 100  $\mu\text{A}/\text{cm}^2$ . The potential scanning direction was reversed when the current density reached 500  $\mu\text{A}/\text{cm}^2$ . Each sample was tested three to five times in the same condition. The error bars show the scatter in the data; unless otherwise stated, if no error bars are visible in a plot, the scatter is smaller than the size of the symbol for the data point.

## Results

### Alloys with 7:3 Ni-Cu Ratio

The corrosion potentials ( $E_{\text{CORR}}$ ), breakdown potentials, ( $E_{\text{B}}$ ), and in some cases the repassivation potentials ( $E_{\text{RP}}$ ) were determined for the various alloys tested. The ultimate goal of this exercise, according to the design criteria mentioned above, is to maximize the  $E_{\text{B}}$  and  $E_{\text{RP}}$  values, hopefully approaching that of 304L SS, about 280 mV<sub>SCE</sub> in 0.1 M NaCl, and to achieve a value of  $E_{\text{CORR}}$  that is slightly noble to that of 304L SS, which is about -140 mV<sub>SCE</sub> in this solution.

Homogenized buttons having Cu content from 25 - 45 wt% were tested in aerated 0.1M NaCl solution. The previous paper reports the behavior of these samples in seawater<sup>1</sup>. As shown in Figure 1, the breakdown potential ( $E_{\text{B}}$ ) of Ni-Cu alloys decreased significantly with the increase of Cu content, but there was very little effect on the corrosion potential ( $E_{\text{CORR}}$ ). The standard electrode potentials of Cu/Cu<sup>2+</sup> and Cu/Cu<sup>+</sup> are 0.340 and 0.522 V<sub>NHE</sub> (Volt vs. Normal Hydrogen Electrode), respectively, both of which are much higher than that for Ni/Ni<sup>2+</sup>, which is -0.23 V<sub>NHE</sub><sup>48</sup>. So it is interesting that the addition of Cu did not contribute much to the ennoblement of the corrosion potential. The effect of Cu in decreasing the  $E_{\text{B}}$  in aerated 0.1M NaCl solution was also observed in seawater<sup>1</sup>.

$E_{\text{B}}$  of Ni-30Cu increased by 50 mV when Mo was added up to 2 wt%, but further Mo additions resulted in drastic decreases in  $E_{\text{B}}$ , Figure 2.  $E_{\text{CORR}}$  decreased slightly but continuously with Mo addition. For improvement of the breakdown behavior of Ni-30Cu alloy, the content of Mo should be controlled to less than 2 wt%. There was no difference in either  $E_{\text{CORR}}$  or  $E_{\text{B}}$  for furnace-cooled samples compared to water-quenched samples of the same composition. This indicates that Mo is not involved in the formation of intermetallic compounds with Ni and Cu, which is expected from its high solubility in Ni-Cu alloy<sup>32-36</sup>.

Pd content had a marked beneficial effect on both  $E_{\text{B}}$  and  $E_{\text{CORR}}$ . The breakdown potential increased by over 60 mV and the corrosion potential by almost 100 mV as the Pd content increased to 2 wt%, Figure 3. The addition of only 1 wt% Pd was sufficient to increase  $E_{\text{CORR}}$  above that for SS 304L. On the other hand, the values of  $E_{\text{B}}$  were still lower than that for SS 304L. The effect of the cooling rate for Pd-containing Ni-Cu alloy was different than that found for other alloying elements. The furnace-cooled samples exhibited higher  $E_{\text{CORR}}$  and  $E_{\text{B}}$  than those of water-quenched samples. Pd has an FCC structure, as do Ni and Cu<sup>11</sup>, so it could be completely soluble. It is possible that Pd segregated at the sample surface, but surface analysis was not performed and it is not clear why the slowly-cooled samples showed this difference.

The combined effects of Mo and Pd are given in Figures 4 and 5.  $E_{\text{B}}$  decreased continuously as Mo was added up to 5 wt% in Ni-30Cu-1Pd, while  $E_{\text{CORR}}$  did not change, Figure 4. The value of  $E_{\text{B}}$  for Ni-30Cu-1Pd and Ni-29Cu-2Mo were both about 120 mV<sub>SCE</sub>, but  $E_{\text{B}}$  for Ni-29Cu-1Pd-1Mo was only about 100 mV; no synergism between the

two alloying elements was found. The furnace-cooled samples showed a little higher  $E_B$  than that of water-quenched samples, which was the same trend found in Ni-Cu alloys with only Pd added.  $E_B$  increased only slightly with the addition of Pd up to 3 wt% in Ni-30Cu-1Mo, Figure 5, so Mo seems to degrade the beneficial effects of Pd on breakdown behavior. However, the ennobling effects of Pd were still evident as  $E_{CORR}$  increased up to  $-30 \text{ mV}_{SCE}$ .

To examine the effects of dilution, additions of Fe and Cr were tested individually and together. Addition of Fe to Ni-30Cu had very little effect on  $E_{CORR}$ , Figure 6.  $E_B$  increased with the addition of 10 wt% Fe, but then decreased with further addition. It is not clear why a small addition of Fe would improve the breakdown behavior of Ni-30Cu. The values of  $E_B$  for the furnace-cooled samples were all about 50 mV lower than those for the water quenched samples of the same composition, which suggests that corrosion-sensitive intermetallic phases containing Fe formed during slow cooling. This was expected by the low solubility of Fe in Ni-Cu system<sup>42, 43, 44</sup>.

The addition of only 3 wt% Cr resulted in a substantial increase in  $E_B$ , but for the water-quenched sample further additions had no effect, Figure 7. Again the breakdown potentials for the furnace-cooled samples were lower than for the water-quenched samples because Cr also could be involved in the formation of intermetallic compounds owing to its low solubility in Ni-Cu alloys<sup>40, 41</sup>. Cr additions resulted in a slight reduction in  $E_{CORR}$  for the water-quenched alloys, and somewhat larger reductions for the furnace-cooled alloys.

Homogenized buttons containing both Fe and Cr were tested as a means of simulating the effect of dilution by stainless steel. However, the Fe:Cr ratio in this series of samples was not always the value in 304 stainless steel, which is 4:1. For those samples, dilution was determined by the sum of the Cr and Fe contents. As the level of dilution increased to 15%,  $E_{CORR}$  decreased slightly but  $E_B$  increased by almost 100 mV for the water-quenched samples, Figure 8. As the level of dilution increased further,  $E_{CORR}$  for the water-quenched samples increased up to  $-50 \text{ mV}_{SCE}$ , but  $E_B$  decreased over this range. The values of  $E_{CORR}$  and  $E_B$  for furnace-cooled samples were lower than for water-quenched, as was generally the case for separate addition of Fe or Cr. The  $E_B$  values for the highest dilutions of 63% for furnace-cooled and of 43% for water-quenched Ni-Cu alloys were 100 and 70  $\text{mV}_{SCE}$ , respectively, which are close to the value for non-diluted Ni-Cu alloys. The separate addition of 10% Fe or 3% Cr, corresponding to about 15% dilution when alloyed together, both resulted in an increase in  $E_B$ , Figures 6 and 7. A further increase in Fe alone decreased  $E_B$ , which suggests that the decrease in  $E_B$  with dilution higher than 15% is caused by the added Fe content. These results suggest that, from a corrosion perspective, dilution levels less than 20% would be preferred when welding stainless steel with Ni-Cu alloys.

Figure 9 shows the results for samples taken from 304L/Monel welds having dilution ranging from 12-63%.  $E_B$  for the real welds decreased slightly as the level of dilution increased, which is the same trend observed in homogenized buttons with changing dilution. However, the values of  $E_B$  for the real welds were 50-100 mV lower. The

$E_{CORR}$  values for these weld samples were scattered in the range of  $-140$  to  $-190$  mV<sub>SCE</sub>, Figure 9. The differences in  $E_B$  and  $E_{CORR}$  for the real welds and the homogenized buttons occur because of the metallurgical heterogeneities in welds, such as concentration gradients in the form of coring in the dendrite<sup>49</sup>, the segregation of specific element at the boundary of dendrites<sup>50</sup>, and the possible formation of a Fe-rich phase<sup>51</sup>.

Figure 10 summarizes the breakdown potentials of buttons of Ni-30Cu with varying levels of dilution and welds made with Monel weld wire. Data for buttons in both the as-cast and homogenized conditions and welds in the as-welded and homogenized conditions<sup>1</sup> are given. The breakdown potentials for homogenized samples are much higher than for samples in the as-cast or as-welded conditions. The Ni-Cu binary system is an ideal substitutional solution, with complete solubility over the whole compositional range<sup>43</sup>. Thus, during non-equilibrium solidification Cu is enriched in the liquid and depleted in the solid, resulting in coring. It was reported that dendrite coring can be homogenized by cold rolling and subsequent annealing<sup>49</sup>. The improved behavior of the homogenized samples indicates that low Cu alloys should be considered. Figure 1 showed that  $E_B$  increased by 100 mV and  $E_{CORR}$  decreased by less than 10 mV when the content of Cu decreased from 30 to 20 wt%. In the subsequent work, attention was focused on samples with lower Cu content.

#### As-Cast Buttons with Low Cu Content

As-cast Ni-Cu buttons with Cu content from 0 - 30 wt% were tested in aerated 0.1 M NaCl, Figure 11. The behavior of samples representing the same alloys with 25% dilution is also shown, as are the data for type 304L SS. For alloys with no dilution, the  $E_{CORR}$  increased by about 70 mV when 5 wt% Cu was added to Ni, and further additions of Cu had little effect. The values of  $E_{CORR}$  for the Cu-containing alloys were all slightly below that of type 304L SS. The alloys with 5 or 10 wt% Cu exhibited the highest  $E_B$  and repassivation potentials ( $E_{RP}$ ), although the increase in  $E_{RP}$  with the addition of 5 wt% Cu relative to pure Ni was much higher than the increase in  $E_B$ . The  $E_B$  values for the Ni-Cu alloys were all lower than that for type 304L SS, but their repassivation potentials were all much higher. The nobility of Cu apparently plays an important role in improving the pit repassivation behavior. Dilution of the alloys with type 304L SS by 25% decreased both  $E_B$  and  $E_{RP}$  for alloys in range of 5-10% Cu, which might be caused by the formation of intermetallic compounds containing Fe and Cr. For samples with 25% dilution, the highest  $E_B$  was for pure Ni, but Cu additions still resulted in a large increase in  $E_{RP}$ . Very little difference in  $E_{CORR}$  was found with Cu concentration for the diluted samples.

From these results it seems that the best Ni-Cu alloys to use for welding of SS contain 5-10 wt% Cu as they exhibit the best combination of breakdown, repassivation, and corrosion potentials. The repassivation potentials are much higher than that of SS304L, but the breakdown potentials are much lower and the corrosion potentials are also lower. As a result, it is of interest to explore the effects of additional alloying.

The behavior of Ni-5Cu alloys with 1 wt% Pd, 3 wt% Mo, or both 1 wt% Pd and 3 wt% Mo is summarized in Figure 12. The effects of 25 and 50% dilution on these alloys are

also shown. The values of  $E_B$ ,  $E_{CORR}$ , and  $E_{RP}$  for almost every level of dilution were highest for the alloy with 1 wt% Pd.  $E_{CORR}$  and  $E_{RP}$  for the 1 wt% Pd were higher than those of type 304L stainless steel for all dilution levels, but  $E_B$  was still lower by 70-100 mV. Mo addition of 3 wt% was only beneficial at the very high dilution of 50%, but it exhibited the lowest  $E_{RP}$  and  $E_{CORR}$  at almost all dilution levels. The addition of both Mo and Pd resulted in values between those for the Ni-Cu alloys alloyed with only Pd and only Mo. The same trends of alloying elements on the  $E_B$ ,  $E_{CORR}$ , and  $E_{RP}$  values were also found for the Ni-10 wt% Cu base alloy, Figure 13. The values of these potentials were almost identical for Ni-5Cu-1Pd and Ni-10Cu-1Pd alloys at all levels of dilution from 0-50%.

### Discussion

A new alloy to be used as a Cr-free consumable for welding of stainless steels requires many properties, such as mechanical strength and ductility, weldability, and corrosion resistance. In this study we have considered only the corrosion properties in searching for an optimized composition. The alloy Ni-(5~10)Cu-1Pd meets the design criteria for a Cr-free welding consumable for 304L stainless steel stated in the introduction; it has a breakdown potential above the corrosion potential of type 304L SS and a corrosion potential slightly above that of type 304L SS. Furthermore, it has the highest breakdown and repassivation potentials of the alloys studied, and a repassivation potential that is significantly higher than that of type S304L stainless steel. These relationships are clearly seen in Figure 14, which is a comparison of representative cyclic polarization curves for the optimized alloy Ni-10Cu-1Pd alloy, Monel K-400, type 304L stainless steel, and a conventional 304L/308L weld in aerated 0.1 M NaCl. The NiCuPd alloy exhibits an increase in the passive current density at around 70 mV<sub>SCE</sub>, but the same  $E_B$  as the 304L/308L weld according to the definition of breakdown potential used in this study. This value of  $E_B$  is about 100 mV below the value for 304L. Furthermore, the  $E_{RP}$  for the alloy is seen to be much higher than the values for 304L or the 304L/308L weld.

The addition of Pd certainly results in a significant increase in material cost, but it provides substantial benefit. It should be noted that Pd contents less than 1 wt% have not yet been studied, and it is possible that smaller Pd contents also provide suitable enhancements in properties. Pd has been known to be a non-reactive element in many environments, and very effective as a hydrogenation catalyst.<sup>11</sup> As Tomashov found for many alloy systems<sup>12</sup>, the addition of Pd to Ni-(5-10)Cu-1Pd also resulted in ennoblement of  $E_{CORR}$ . This might be caused by a high exchange current density for the reduction reaction<sup>18</sup>. The beneficial effects of Pd on localized corrosion might be related to enrichment on the surface of actively growing pits. Pd has also been shown to exhibit some synergetic effect with Mo in pure Cr<sup>14-16</sup>, but no such synergism was exhibited in the Ni-Cu alloys.

Cu showed both beneficial and detrimental effects on the breakdown behavior of Ni-Cu alloys. It has been reported that Cu improved the self-healing of localized attack during long term exposure because of its high reversible potential<sup>48</sup>, but it was also observed that Cu was selectively dissolved in Cl<sup>-</sup> environment<sup>6,8</sup> and degraded the passivity<sup>4</sup>. In this study, the specific role of Cu on the passivity and its breakdown was not clear, but the

best resistance to the breakdown of passivity was found in range of 5-10 wt% Cu. The large benefit of Cu in increasing the repassivation potential could be related to enrichment of Cu within pits, which results in a form of self-healing of the localized attack.

Even though Mo has been known to promote corrosion resistance in Ni alloys<sup>21,22</sup>, its addition to Ni-Cu alloys in this study degraded the resistance to the localized corrosion. As shown in Figure 2 a small amount of Mo addition, less than 2 wt%, did increase  $E_B$ , but Mo obstructed the beneficial effect of Pd when both elements were added. This detrimental effect of Mo on passivity was also found for pure Ni and Fe<sup>24</sup>, and was attributed to increased Ni-site vacancies by the doping effect of Mo in the NiO film and enhanced dissolution<sup>25, 26, 30</sup>.

Dilution is an important factor in real welds as some amount of the base metal will end up in the weld metal, and the transition zone contains a gradient region with dilution up to 100% base metal. The addition of Fe and Cr in homogenized Ni-Cu alloys changed the breakdown behavior even for small amount of each element. Cooling rate also affected the breakdown behavior, which might have been associated with the formation of intermetallic compounds because of low solubility of Fe and Cr in Ni-Cu alloys<sup>40-43,44</sup>.

Micro-segregation of Cu at dendrite boundaries formed during solidification of the buttons or a weld can also affect the corrosion resistance. In the ideal Ni-Cu binary system<sup>43</sup>, the maximum difference of Cu content between Cu-enriched liquid and Cu-depleted solid during equilibrium solidification is about 10 at% for Ni-29 at% Cu (Ni-30 wt% Cu). For non-equilibrium cooling, this difference could be frozen into a cored structure. According to the data shown in Figure 1, a difference in Cu content of 10 at% could be sufficient to change the localized corrosion behavior of Ni-Cu alloys. The difference in  $E_B$  between homogenized and as-cast buttons of Ni-30Cu alloys shown in Figure 10 can be explained by this segregation effect. However, for Ni-10Cu, the difference of Cu content between liquid and solid is just 3 at%, which should not have a large effect on the breakdown behavior. So the segregation should be minimized in the optimized alloy containing 5-10 wt% Cu.

The effects of each element studied on  $E_{CORR}$ ,  $E_B$ , and  $E_{RP}$  for Ni-Cu alloys are summarized in Table 4. Cu increased the corrosion potential, but degraded the passivity and its breakdown. Pd had a strong ennobling effect and improved the localized corrosion resistance. Mo was not beneficial to any aspect of the corrosion properties. The effects of Fe and Cr on the formation of secondary phases and on the corrosion resistance of the Ni-Cu alloys are not fully clear. Fe and Cr can change the corrosion resistance of the Ni-Cu alloys by themselves and also by the formation of secondary phases during solidification. Considering corrosion properties only, dilution should be kept to the range of less 20%.

Successful application of this alloy as a practical consumable for welding of stainless steel will require further investigations into weldability, mechanical properties, and

corrosion behavior in a range of environments, including more oxidizing environments. Subsequent reports will describe the results of these investigations<sup>52</sup>.

### Conclusions

Ni-Cu alloys containing other minor alloying element additions were studied in aerated 0.1 M NaCl to develop a material with suitable corrosion properties for use as a Cr-free consumable for welding type 304L stainless steel. The following was observed:

- The addition of 5~10wt% Cu to Ni improved the resistance to localized corrosion.
- Pd additions in the range of 1-2% had a large influence in ennobling the  $E_{CORR}$  and improving the localized corrosion behavior of Ni-Cu alloys.
- The addition of Mo was not effective for improving the breakdown behavior of Ni-Cu alloys.
- The addition of up to 10 wt% Fe improved the breakdown behavior of Ni-Cu alloy, but larger amounts of Fe decreased  $E_B$ . Slow-cooling of Ni-Cu alloys containing Fe degraded the localized corrosion resistance.
- Cr addition increased  $E_B$  but slightly decreased  $E_{CORR}$ . The addition of more than 3 wt% Cr did not further improve the breakdown behavior, but slow-cooling degraded the localized corrosion resistance.
- Dilution of Ni-Cu with stainless steel up to 15% improved the localized corrosion resistance, but slightly decreased  $E_{CORR}$ . Further dilution degraded the corrosion resistance.
- Low heat input and fast cooling rate should minimize the deleterious segregation and dilution effects on the corrosion properties of a weld made with a Ni-Cu consumable.
- The optimized composition for a new Cr-free consumable for welding type 304 stainless steel is Ni-(5~10)Cu-1Pd.  $E_{CORR}$  of this alloy in 0.1M NaCl was slightly higher than that of type 304L stainless steel. The  $E_B$  of this alloy was slightly lower than that of conventional weld made with 308L filler metal, but its  $E_{RP}$  was much higher.

### Acknowledgements

This work was supported by SERDP (Strategic Environmental Research and Development Program) through project PP-1346 and under the direction of C. Pellerin.

### References

1. Y. H. Kim, G. S. Frankel, J. C. Lippold and G. Guaytima, to be submitted to Corrosion.
2. G. N. Flint and W. Barker, in Society of Chemical Industry, held Oct. 21, 1964 (London, England, Chemical Engineering Group) p. FB1.
3. S. Masaki and K. Hirano, Bosei Kanri 35, 1 (1991) p. 25.

4. E. D. Verink Jr. and I. T. S. Lee, in Third International Congress on Marine Corrosion and Fouling, held Oct. 2-6, 1972 (Gaithersburg, Maryland, USA, National Bureau of Standards) p. 241.
5. O. Tajima and K. Nakao, Technology Reports of Kansai University 16, (1975) p. 123.
6. A.-M. Beccaria and J. Crousier, British Corrosion Journal 24, 1 (1989) p. 49.
7. A. Azzam, A. A. Abdel-Fattah, H. E. Megahed and A. Y. Eletre, J. Electrochem. Soc. India 49, 1 (2000) p. 7.
8. R. B. Niederberger, R. J. Ferrara and F. A. Plummer, Materials Protection and Performance 9, 8 (1970) p. 18.
9. R. B. Niederberger, R. J. Ferrara and F. A. Plummer, in 26th Conference of National Association of Corrosion Engineers, held Mar. 2-6, 1970 (Philadelphia, PA, NACE) p. 188.
10. A. M. Zaky and F. H. Assaf, British Corrosion Journal 37, 1 (2002) p. 48.
11. J. Edwards, Coating and Surface Treatment Systems for Metals (Redwood Books Ltd., Trowbridge, UK, 1994) p.102.
12. N. D. Tomashov and G. P. Chernova, Passivity and protection of Metals against Corrosion, translated by B. H. Tytell, ed. by H. H. Uhlig (Plenum Press, New York, 1967) p. 82.
13. T. P. Hoar, Platinum Metals Review 2, 4 (1958) p. 117.
14. P. L. Andresen, S. Hettiarachchi, Y. J. Kim, and T. P. Diaz, Co-deposition of palladium during oxide film growth in high-temperature water to mitigate stress corrosion cracking, Patent No. US5608766, (General Electric Co., USA, 1997)
15. P. L. Andresen, S. Hettiarachchi, Y. J. Kim, and T. P. Diaz, Co-deposition of palladium during oxide film growth in high-temperature water to mitigate stress corrosion cracking, Patent No. US5768330 (General Electric Co., USA, 1998).
16. P. L. Andresen, in Sixth International Symposium on Environmental Degradation of Materials in Nuclear Power Systems - Water Reactors, held Aug. 1-5, 1993 (San Diego, CA, TMS) p. 245.
17. S. Hettiarachchi, Palladium acetylacetonate solution and related method of manufacture, Patent No. US5448605 (General Electric Co., USA, 1995).
18. J. H. Potgieter, Journal of the Applied Electrochemistry 21, (1991) p. 471.

19. P. Peled and D. Itzhak, *Corrosion Science* 32, 1 (1991) p. 83.
20. G. P. Chernova, T. A. Fedoseeva, L. P. Kornienko and N. D. Tomashov, *Surface Technology* 13, (1981) p. 241.
21. R. W. Revie, *Uhlig's Corrosion Handbook* (John Wiley & Sons, Inc., Pennington, 2000).
22. A. I. Asphahani, in *Metals Handbook*; Vol. 13, 9th ed., edited by L. J. Korb (ASM International, Metals Park, Ohio, 1987), p. 641.
23. E. Beltowska-Lehman, *Surface and Coating Technology* 151-152, (2002) p. 440.
24. A. V. Plaskeev and V. M. Knyazheva, *Protection of Metals* 31, 1 (1995) p. 42.
25. V. Mitrovic-Scepanovic and M. B. Ives, *J. Electrochem. Soc.* 127, 9 (1980) p. 1903.
26. V. Mitrovic-Scepanovic and M. B. Ives, *Corrosion* 40, 12 (1984) p. 655.
27. D. D. MacDonald, M. Ben-Haim and J. Pallix, *Corrosion Science* 31, (1990) p. 223.
28. S. Kato, S. Takagi, M. Kawasaki, K. Mori and K. Ueda, *Corrosion-resistant alloy for build-up welding, JP5082625*, (Jpn. Kokai Tokkyo Koho, 1992).
29. M. Moriya and M. B. Ives, *Corrosion* 40, 3 (1984) p. 105.
30. R. Cortes, M. Froment, A. Hugot-Le Goff and S. Joiret, *Corrosion Science* 31, (1990) p. 121.
31. L. Bosio, R. Cortes, P. Delichere, M. Froment and S. Joiret, *Surface and Interface Analysis* 12, (1988) p. 380.
32. R. F. Kozlova and V. B. Rabkin, *Soviet Powder Metallurgy and Metal Ceramics* 12, 2 (1973) p. 140.
33. R. F. Kozlova, V. B. Rabkin, L. Y. Losev and E. F. Pashchenko, *Soviet Powder Metallurgy and Metal Ceramics* 12, 5 (1973) p. 399.
34. O. K. Teodorovich and M. M. Churakov, *Soviet Powder Metallurgy and Metal Ceramics* 19, 4 (1980) p. 290.
35. K. P. Gupta, *Phase diagrams of ternary nickel alloys* (Indian Institute of Metals, Kanpur, India, 1991) p. 82.
36. K. P. Gupta and S. B. Rajendraprasad, *J. Alloy Phase Diagram* 6, 3 (1990) p. 164.

37. T. Hoshino and M. Asato, in International Conference on Solid-Solid Phase Transformation '99 (JIMIC-3), held May 24-28, 1999 (Kyoto, Japan, The Japan Institute of Metals) p. 629.
38. M. Asato and T. Hoshino, *J. Japan Inst. Metals* 63, 6 (1999) p. 676.
39. T. Hoshino, *Physical Review B* 47, 9 (1993) p. 5106.
40. V. M. Lopez-Hirata, F. Hernandez-Santiago, H. Dorantes-Rosales, M. L. Saucedo-Munoz and J. M. Hallen-Lopez, *Materials Transactions* 42, 7 (2001) p. 1417.
41. K. P. Gupta, S. B. Rajendraprasad, A. K. Jena and R. C. Sharma, *J. Alloy Phase Diagram* 1, 9 (1985) p. 39.
42. V. M. Lopez-Hirata, N. Sano, T. Sakurai and K. Hirano, *Acta metall. mater.* 41, 1 (1993) p. 265.
43. M. Hasebe and T. Nishizawa, in *Application of Phase Diagrams in Metallurgy and Ceramics*, held Jan. 10-12, 1977 (Gaithersburg, MD, National Bureau of Standards) p. 911.
44. K. C. Harikumar and V. Raghavan, *J. Alloy Phase Diagram* 5, 3 (1989) p. 201.
45. J. F. Counsell, E. B. Lees and P. J. Spencer, in *Metallurgical Chemistry*, held Jul. 14-16, 1971 (London, England, National Physical lab.) p. 3.
46. G. W. Qin, G. Zhao, M. Jiang, H. X. Li and S. M. hao, *Z. Metallkd* 91, 5 (2000) p. 379.
47. R. P. Wahi and J. Stajer, in *2nd Acta-Scripta Metallurgica Conference - Decomposition of Alloys : The Early Stages*, held Sep. 19-23, 1983 (Sonnenberg, Germany) p. 165.
48. A. J. Bard and L. R. Faulkner, *Electrochemical Methods : Fundamentals and Applications* (John Wiley & Sons, New York, 1980) p. 700.
49. B. Prakash, *J. Electrochem. Soc. India* 27, 2 (1978) p. 101.
50. M. J. Perricone and J. N. Dupont, in *Materials Solutions 2001 on Joining of Advanced and Specialty Materials*, held Nov. 5-8, 2002 (Indianapolis, IN, ASM International) p. 22.
51. G. Newcombe, *Welding and metal fabrication* 42, 10 (1974) p. 379.
52. Y. H. Kim, G. S. Frankel and J. C. Lippold, to be submitted to *Corrosion* (2005).

Table 1. The level of dilution by different heat input of GTAW procedure

No.	Heat input rate (KJ/in)	Level of Dilution (%)	Remark
1	20	13	
2*	24	12	
3	24	24	
4	36	43	Solidification crack occurred
5	42	53	
6	42	60	Solidification crack occurred

\* Multipass welding

Table 2. Composition of 7:3 Ni-Cu alloys. Samples were fabricated by electric-arc melting, cold-rolling, annealing for homogenization, and either water quenching or furnace cooling.

No.	Alloying chemistry (wt%)						Dilution Level (%)	Remark
	Ni	Cu	Pd	Mo	Fe	Cr		
1	70	30	0	0	0	0	0	Basic chemistry
2	69.3	29.7	0	1.0	0	0	0	Mo effect
3	68.6	29.4	0	2.0	0	0	0	Mo effect
4	66.5	28.5	0	5.0	0	0	0	Mo effect
5	63.0	27.0	0	10.0	0	0	0	Mo effect
6	69.3	29.7	1	0	0	0	0	Pd Effect
7	68.6	29.4	2	0	0	0	0	Pd Effect
8	68.6	29.4	1	1	0	0	0	Mo & Pd Effect
9	65.8	28.2	1	5	0	0	0	Mo & Pd Effect
10	67.2	28.8	3	1	0	0	0	Pd & Mo effect
11	63.0	27.0	0	0	10	0	0†	Fe effect
12	56.0	24.0	0	0	20	0	0†	Fe effect
13	49.0	21.0	0	0	30	0	0†	Fe effect
14	67.9	29.1	0	0	0	3	0†	Cr effect
15	66.5	28.5	0	0	0	5	0†	Cr effect
16	63.0	27.0	0	0	0	10	0†	Cr effect
17	60.9	26.1	0	0	10	3	13	Fe & Cr effect
18*	59.5	25.5	0	0	10	5	15	Fe & Cr effect
19	52.5	22.5	0	0	20	5	25	Fe & Cr effect
20	42.0	18.0	0	0	30	10	40	Fe & Cr effect
21	32.9	14.1	0	0	40	13	53	Fe & Cr effect
22	23.1	9.9	0	0	50	17	67	Fe & Cr effect
23	80	20	0	0	0	0	0	Cu effect
24	79.2	19.8	1	0	0	0	0	Cu & Pd effect

\*The Fe:Cr ratio is lower than that of SS304L

† addition of Fe or Cr alone does not simulate dilution by type 304L stainless steel

Table 3. Composition of low-Cu Ni-Cu alloys. Samples were fabricated by electric-arc melting and tested in as-cast condition with no further processing.

No.	Alloying chemistry (wt%)							Dilution Level (%)	Remark
	Ni	Cu	Pd	Mo	Fe	Cr	SS*		
25	100	0	0	0	0	0	0	0	Effect of Cu
26	95	5	0	0	0	0	0	0	Effect of Cu
27	90	10	0	0	0	0	0	0	Effect of Cu
28	85	15	0	0	0	0	0	0	Effect of Cu
29	80	20	0	0	0	0	0	0	Effect of Cu
30	91	5	1	3	0	0	0	0	Ni-5Cu-1Pd-3Mo
31	92	5	0	3	0	0	0	0	Ni-5Cu-3Mo
32	94	5	1	0	0	0	0	0	Ni-5Cu-1Pd
33	70.5	3.7	0.8	0	-	-	25	25	Ni-5Cu-1Pd(25% dil.)
34	47	2.5	0.5	0	-	-	50	50	Ni-5Cu-1Pd(50% dil.)
35	86	10	1	3	0	0	0	0	Ni-10Cu-1Pd-3Mo
36	87	10	0	3	0	0	0	0	Ni-10Cu-3Mo
37	89	10	1	0	0	0	0	0	Ni-10Cu-1Pd
38	66.7	7.5	0.8	0	-	-	25	25	Ni-10Cu-1Pd(25% dil.)
39	44.5	5	0.5	0	-	-	50	50	Ni-10Cu-1Pd(50% dil.)

\*SS : Type 304L stainless steel chips used.

Table 4. Summary of the effect of alloying elements on the corrosion of Ni-Cu alloys

	Cu	Pd	Mo	Fe	Cr	Dilution
$E_{CORR}$	+	++	-	0	-	+
$E_B$	-	++	--	0	+	+
$E_{RP}$	-	++	0	0	-	-

+ : increase, - : decrease, 0 : no effect

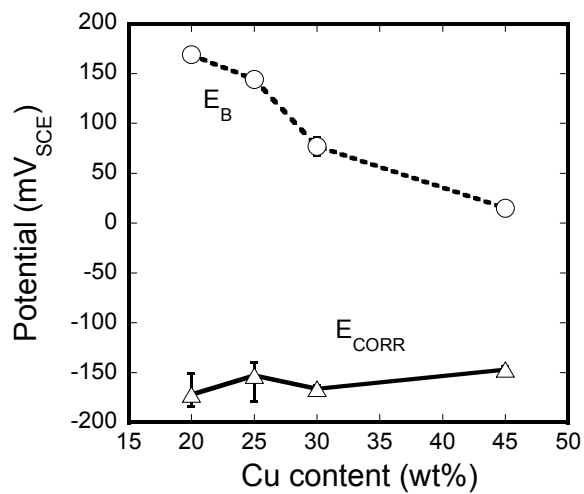


Figure 1. The effect of Cu content on the  $E_{CORR}$  and  $E_B$  of furnace-cooled Ni-Cu alloys in aerated 0.1 M NaCl.

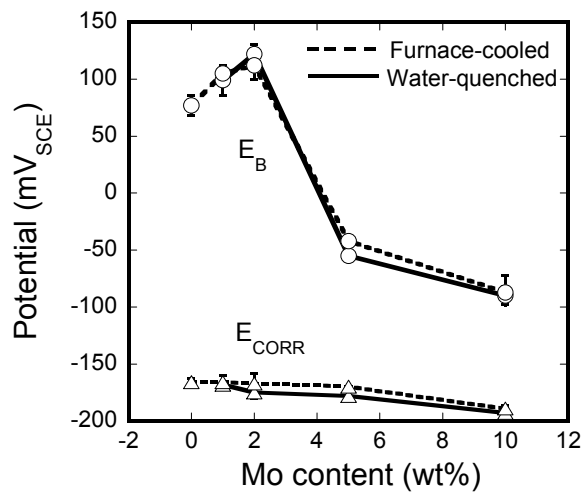


Figure 2. The effect of Mo content on the  $E_{CORR}$  and  $E_B$  of furnace-cooled and water-quenched 7:3 Ni-Cu alloys in aerated 0.1 M NaCl.

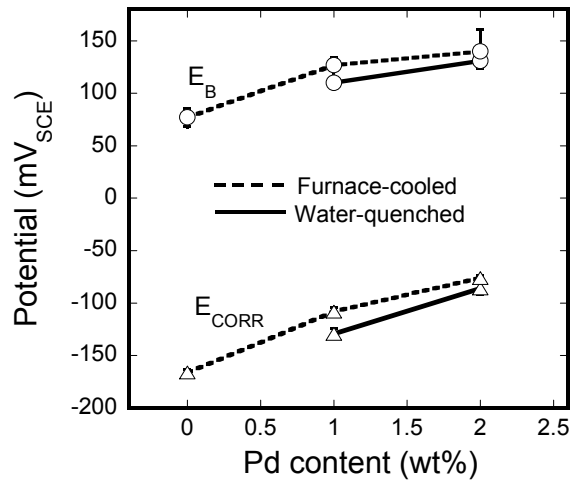


Figure 3. The effect of Pd content on the  $E_{CORR}$  and  $E_B$  of furnace-cooled and water-quenched 7:3 Ni-Cu alloys in aerated 0.1 M NaCl.

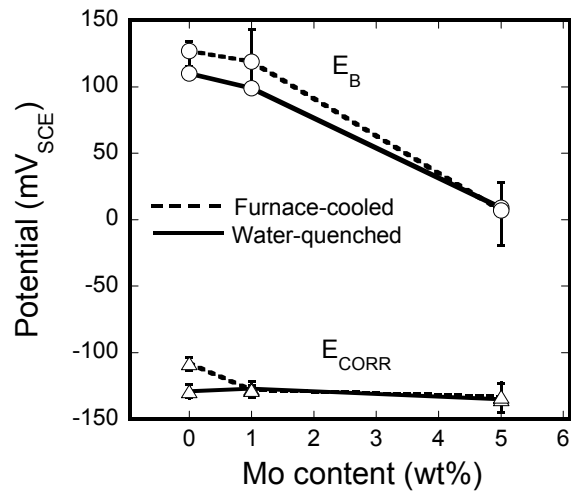


Figure 4. The effect of Mo content on the  $E_{CORR}$  and  $E_B$  of furnace-cooled and water-quenched 7:3 Ni-Cu alloys with 1 wt% of Pd in aerated 0.1 M NaCl.

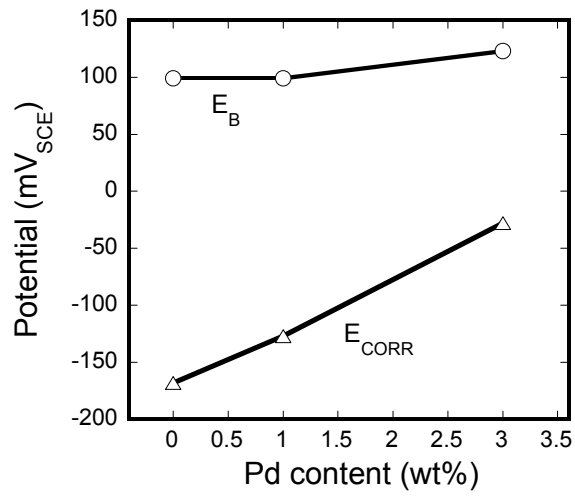


Figure 5. The effect of Pd content on the  $E_{CORR}$  and  $E_B$  of water-quenched 7:3 Ni-Cu alloys with 1 wt% Mo in aerated 0.1 M NaCl.

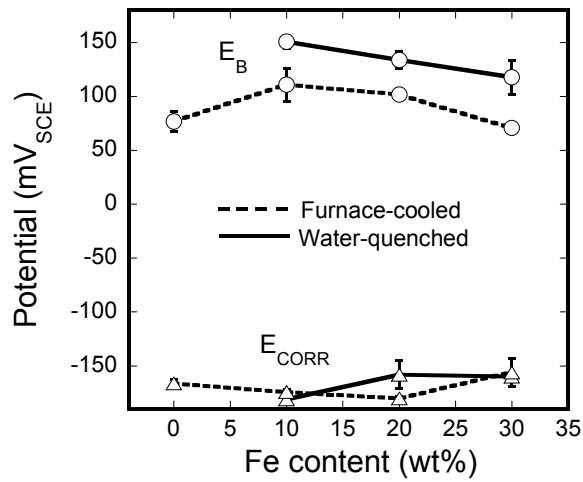


Figure 6. The effect of Fe content on the  $E_{CORR}$  and  $E_B$  of furnace-cooled and water-quenched 7:3 Ni-Cu alloys in aerated 0.1 M NaCl.

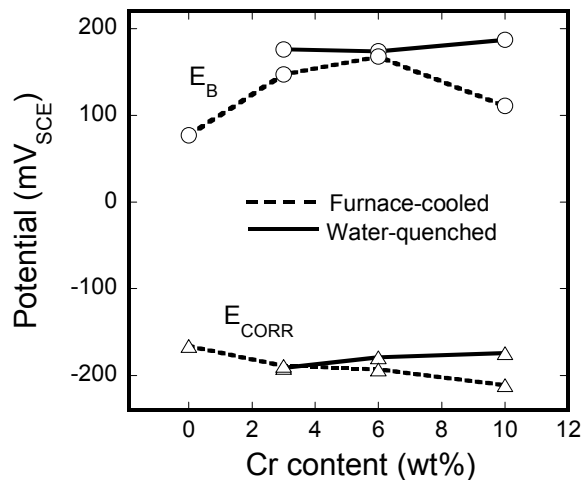


Figure 7. The effect of Cr content on the  $E_{CORR}$  and  $E_B$  of furnace-cooled and water-quenched 7:3 Ni-Cu alloys in aerated 0.1 M NaCl.

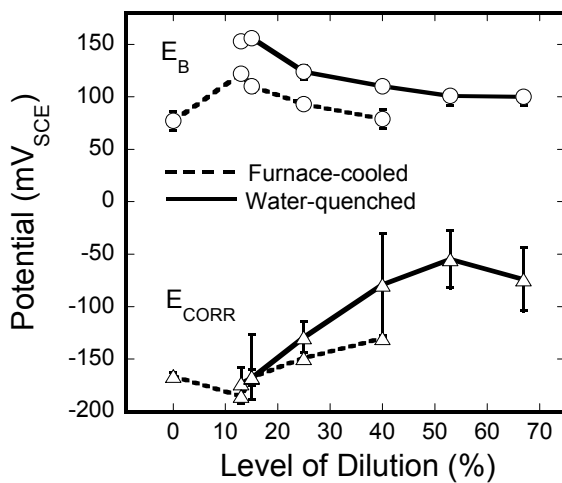


Figure 8. The effect of dilution on the  $E_{CORR}$  and  $E_B$  of furnace-cooled and water-quenched 7:3 Ni-Cu alloys in aerated 0.1 M NaCl.

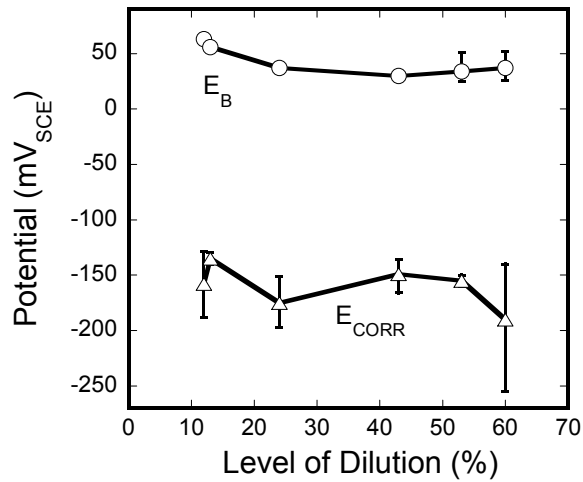


Figure 9. The effect of dilution on the  $E_{CORR}$ (a) and  $E_B$ (b) of 304L/Monel welds in aerated 0.1 M NaCl.

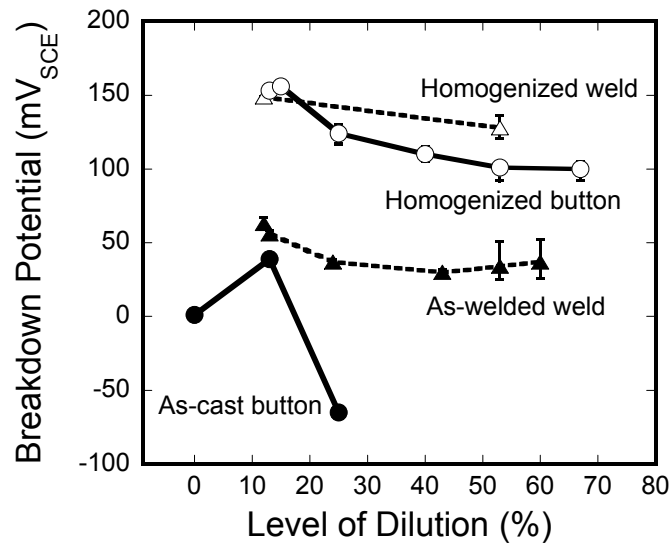


Figure 10. The comparison on the differences of the  $E_B$  of non-homogenized and homogenized 304L/Monel welds<sup>1</sup> and 7:3 Ni-Cu alloy buttons in aerated 0.1 M NaCl. Note that only one sample was tested for each level of dilution for the as-cast buttons.

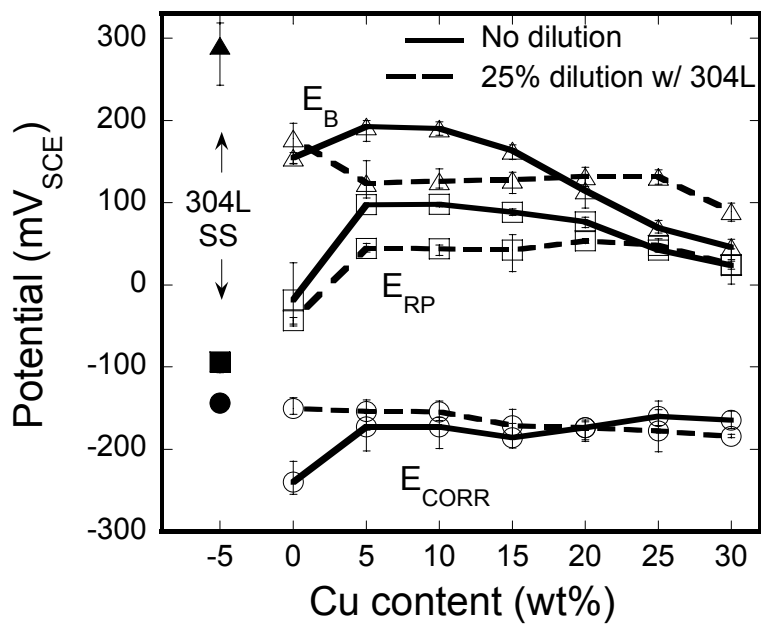
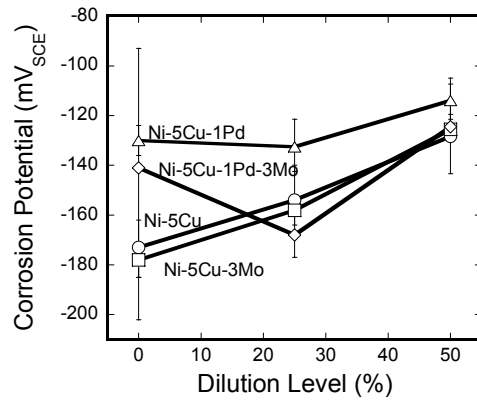
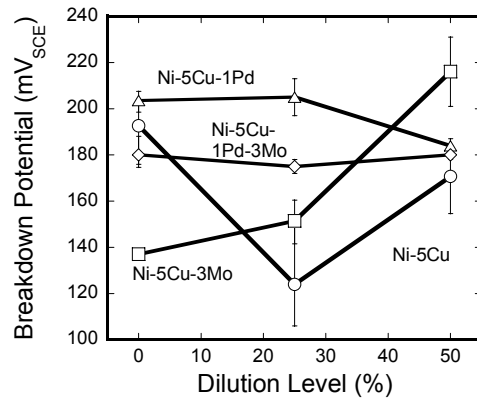


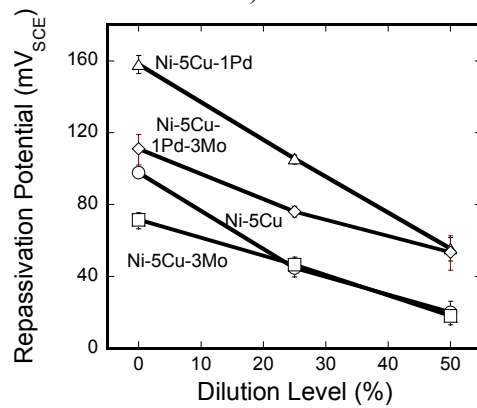
Figure 11. The effect of Cu content on the  $E_{CORR}$ ,  $E_B$ , and  $E_{RP}$  of as-cast Ni-Cu alloys with and without 25% dilution in aerated 0.1M NaCl. The values for type 304L stainless steel are shown at left of plot for comparison.



a)

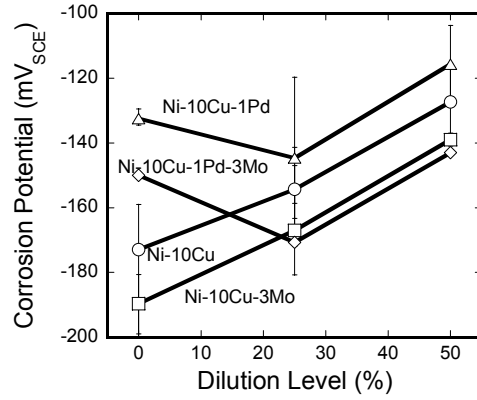


b)

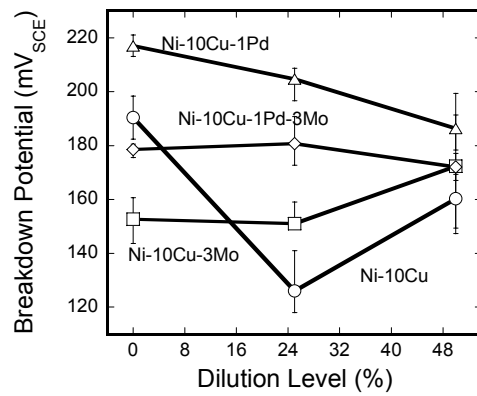


c)

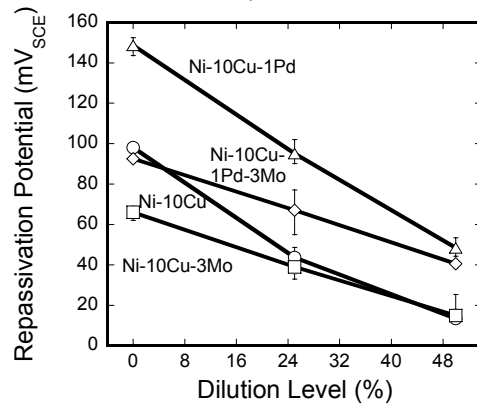
Figure 12. The effect of alloying elements of Pd and Mo on the  $E_{CORR}$ (a),  $E_B$ (b), and  $E_{RP}$ (c) of as-cast Ni-5Cu alloys with the dilution of 0%, 25% and 50% in aerated 0.1 M NaCl.



a)



b)



c)

Figure 13. The effect of alloying elements of Pd and Mo on the  $E_{CORR}$  (a),  $E_B$  (b), and  $E_{RP}$  (c) of as-cast Ni-10Cu alloys with the dilution of 0%, 25% and 50% in aerated 0.1 M NaCl.

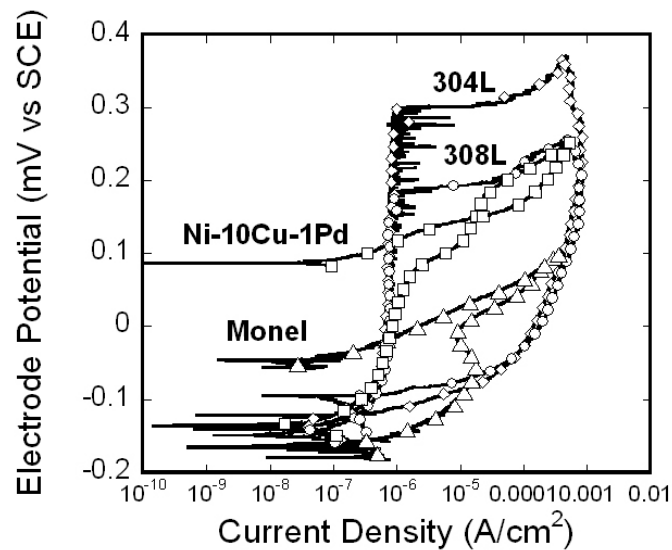


Figure 14. Cyclic polarization behavior of type 304L stainless steel, conventional weld of 308L, as-cast Ni-10Cu-1Pd alloy, and Monel in aerated 0.1 M NaCl.